Atmospheric Environment 330 (2024) 120556

Contents lists available at ScienceDirect

Atmospheric Environment

journal homepage: www.elsevier.com/locate/atmosenv

Sources of wintertime $PM_{2.5}$ at a major city in an Alpine Valley: The role of atmospheric dispersion and inversion dynamics

Mauro Masiol [a,*], Gianni Formenton [b], Flavia Visin [a], Alessandro Bonetto [a], Manuela Rovea [b], Silvia Ficotto [b], Elisa Danesin [a], Tommaso Toffanin [a], Anita Maggiulli [a], Maria Battistel [a], Giovanna Mazzi [a], Matteo Feltracco [a], Andrea Gambaro [a], Philip K. Hopke [a,c,d]

[a] Dept. Environmental Sciences, Informatics and Statistics, Università Ca' Foscari Venezia, Campus Scientifico, Via Torino 155, 30172, Mestre, VE, Italy
[b] ARPAV - Regional Agency for Environmental Protection and Prevention of Veneto, Via Lissa 6, 30174, Mestre, VE, Italy
[c] Dept. Public Health Sciences, University of Rochester Medical Center, Rochester, NY, 14642, USA
[d] Institute for a Sustainable Environment, Clarkson University, Potsdam, NY, 13699, USA

HIGHLIGHTS

- $PM_{2.5}$ sources identified through PMF in a major city in an Alpine valley.
- Biomass burning account for 52% of $PM_{2.5}$, secondary aerosol 21%, biogenic 20%.
- Persistent thermal inversion events identified from high-low altitude weather data.
- Biomass burning and secondary aerosol were higher in all inversion periods.
- Major effort needed to mitigate the biomass burning pollution in mountain valleys.

GRAPHICAL ABSTRACT

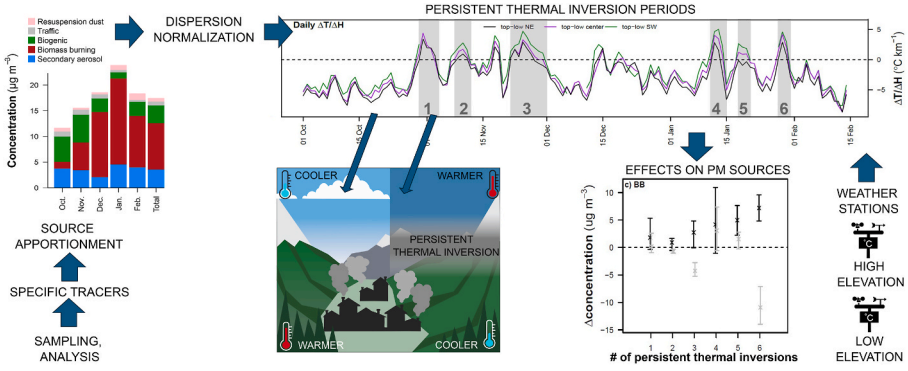

ARTICLE INFO

Keywords:
Particulate matter
Chemical speciation
Source apportionment
Biomass burning
Alpine environment

ABSTRACT

Urban areas in mountain environments are generally located on valley floors surrounded by slopes, where mountain orography drives peculiar meteorology and atmospheric circulation. Also, persistent inversion dynamics may occur strongly affecting air pollution. This study characterizes the $PM_{2.5}$ pollution in a major city located in an Alpine valley (Belluno, Northeastern Italy) during the cold season (Autumn-Winter). Major particulate species (elemental and organic carbon, major inorganic ions) and minor/trace elements conventionally used as tracers for source apportionment were analyzed, including oxalate and specific $PM_{2.5}$-bound tracers for biomass burning (K^+, levoglucosan, mannosan, galactosan) and for primary biogenic organic aerosol (arabitol, mannitol, glucose). $PM_{2.5}$ sources are identified through positive matrix factorization and a series of post-processing tools. Results indicate that biomass burning, mostly emitted by residential wood combustion for domestic heating, is the major source (52% $PM_{2.5}$ mass concentration), followed by secondary aerosol (21%), biogenic aerosol (20%), traffic (4%), and dust resuspension (3%). The source contributions are assessed by accounting for the local meteorology. Insights into the dispersion or buildup of $PM_{2.5}$ sources were then

* Corresponding author.
E-mail address: mauro.masiol@unive.it (M. Masiol).

https://doi.org/10.1016/j.atmosenv.2024.120556
Received 19 March 2024; Received in revised form 20 April 2024; Accepted 29 April 2024
Available online 30 April 2024

investigated by dispersion normalization. In addition, the possible effects of persistent thermal inversion events were evaluated by assessing the inversion strength from temperature profiles measured at multiple weather stations at different elevations with respect to the source contributions. Beyond the identification of those emission sources requiring further mitigation actions, this study also analyses the potential effects of local meteorology on $PM_{2.5}$ pollution. The methodologies applied in this study can be easily adopted to other mountain environments for successful management of air quality.

1. Introduction

Emissions of fine ambient particulate matter ($PM_{2.5}$) dropped in the EU-27 Member States by 28% between 2005 and 2021 (EEA, 2023a) following increasingly stringent policies mandated by the European Union (EU) and the implementation of effective emission control technologies for several major emission source sectors, mostly energy generation, industry, and transport (Turnock et al., 2016). Despite widespread improvements in air quality across Europe (EEA, 2020), particulate pollution still exceeds some EU air quality standards (AQS) (e.g., Directive, 2008/50/EC; EU, 2008) and WHO guidelines (WHO, 2006; 2021) in some hotspots (EEA, 2020; 2023b). The non-attainment of AQS is expected to worsen further by 2030 since more stringent limit values are currently under discussion (EC, 2022) for a better alignment with the new WHO global air quality guidelines (WHO, 2021). The annual average $PM_{2.5}$ limit value will significantly drop from 20 to 10 $\mu g\ m^{-3}$, a limit comparable with US (9 $\mu g\ m^{-3}$) or UK (10 $\mu g\ m^{-3}$). Also, maximum daily concentrations for $PM_{2.5}$ will be introduced: 25 $\mu g\ m^{-3}$ not to be exceeded more than 18 times per calendar year.

These new limit values are challenging to meet. For example, using Bayesian geostatistical regression models, Beloconi and Vounatsou (2023) showed that 47.5% of the total European population lived in areas where the revised EU thresholds were not attained during 2021. Given this issue, the main goal for research and local environmental protection agencies is to identify and quantify the major sources of PM mass. This urgent task is required to successfully plan future emissions reduction actions in time to meet the new AQS.

Northern Italy, particularly the Po Valley, is a known major European hotspot for PM (e.g., EEA, 2020; Masiol et al., 2017; Pivato et al., 2023; Ricciardelli et al., 2017; Scotto et al., 2021). In Veneto, a region encompassing the northeastern part of the Po Valley, numerous source apportionment studies have been conducted in the past decades to identify and quantify the most important sources of PM_{10}, $PM_{2.5}$ and PM_1 at several sites (e.g., Gregoris et al., 2021; Masiol et al., 2012, 2014; Squizzato et al., 2016, 2017; Stortini et al., 2009). However, most of the studies were performed in the surroundings of Venice, the regional capital city. A recent multiple-site study was conducted in 6 major cities across the region: 4 located in the main valley, one in the hilly area facing the valley and one in a mountain valley within the Alpine chain (Masiol et al., 2020). Results indicated common source profiles in all cities except in the mountain city. This difference was attributed to the potentially varying emission source profiles characterizing the mountain areas and differences in local meteorological conditions.

Urban areas in mountain environments are generally located on valley floors surrounded by slopes and are therefore "sheltered" from synoptic-wind systems. Thus, mountain orography drives peculiar meteorological and atmospheric circulation conditions (Whiteman, 2000) that is mostly dependent on local thermal forcing, such as local thermal winds (Cantelli et al., 2017; Giovannini et al., 2014; Gohm et al., 2009). Also, persistent thermal inversions may occur, especially in winter, trapping the pollutants close to the surface (Chazette et al., 2005; Largeron and Staquet, 2016). Additionally, natural and anthropogenic emission sources may differ from the other major cities in the Po Valley. For instance, natural biogenic emissions are expected to be significantly higher due to extended forests and Alpine grasslands as well as to changes in the ratios between anthropized vs. agricultural/natural landscapes. Furthermore, biomass burning (BB) in mountain areas is expected to account for a larger fraction of emissions from domestic heating because of the reduced availability of natural gas (smaller valleys are not connected), the availability of raw material (wood), and the greater propensity of the population to use traditional stoves.

This study characterized the $PM_{2.5}$ pollution in a major city located in an Alpine valley, Belluno (BL), during the cold season (Autumn-Winter), identifying and quantifying the main potential sources. This source apportionment takes advantage of using specific organic tracers for BB and primary biogenic organic aerosol along with major particulate compounds and minor/trace elements conventionally used as tracers. Beyond the indication of which emission sources require further mitigation actions in a typical major Alpine city, this study also analyzes the potential effects of local meteorology on $PM_{2.5}$ pollution. Insight into the dispersion or buildup of pollution sources were investigated by dispersion normalization (Dai et al., 2020) and by identifying periods with persistent thermal inversions.

2. Materials and methods

2.1. Study area

Valbelluna is a large mountain valley extending for ~50 km from NE to SW between the southern Alpine front ranges (pre-Alps) and the Dolomites. The height of surrounding mountains varies from 700 to 2500 m above sea level. It is one of the most populated areas of the Southeastern Alps, hosting around 120,000 inhabitants in two main cities, Belluno at the NE corner of the Valley (altitude 390 m, approx. 35,000 inhabitants over the whole municipality) and Feltre (20,000) at the SW corner, and many smaller towns scattered throughout the valley (Figs. S1a and b). The valley floor is heavily anthropized (Fig. S1c) with (i) major roads, (ii) a railway that is mostly electrified but also uses diesel-powered trains, (iii) small industries, mostly manufacturing home appliances, eyewear, bathroom fixtures, and diary, and (iv) agriculture dominated by cultivated crops and orchards. Although the city is not a main tourist destination, it attracts artistic-cultural tourism and is indirectly linked to Alpine tourism both in winter (skiing) and summer. Beyond local emission sources, atmospheric transport of polluted air masses from neighboring anthropized areas such as the Po Valley represents an additional input of pollution over Alpine environments (Diemoz et al., 2019a; 2019b).

2.2. Analytical

$PM_{2.5}$ was collected at an urban background station (BL, 46°8′30N, 12°13′3E, 394 m a.s.l.) managed by the Regional Environmental Protection Agency (ARPAV). The site is located within an urban green park in the city center (Fig. S1d) representative of city-wide air quality. $PM_{2.5}$ is continuously measured since 2009; in this study, the chemical speciation analysis is limited to October 1, 2020–February 14, 2021. A total of 133 daily samples were collected and weighted according to the UNI EN 12341:2014 standard using quartz fiber filters (Whatman QMA). $PM_{2.5}$ mass was measured gravimetrically (sensitivity $\leq$0.1 μg) with filter blanks and sampled filters conditioned for 48 h at 20 ± 1 °C and 50 ± 5% RH. To prevent positive or negative artifacts for organics and nitrate, photochemical reactions and biological processes, the sampler was kept under controlled temperature and filters were stored in clean Petri slides and refrigerated in the dark until analysis.

A 1 cm^2 punch was analyzed for EC and OC using a carbon aerosol analyzer (Sunset Lab, USA) adopting the EUSAAR2 protocol (Brown et al., 2017; Cavalli et al., 2010) and UNI EN 16909:2017. Two or three 1.5 cm^2 punches were extracted in ultrapure water (specific resistivity 18.2 MΩ cm) for 10 min under controlled temperature (20 °C) and then filtered through 0.22 μm PTFE filter disks. Aliquots of water-dissolved samples were analyzed for (i) major cations (Na^+, NH_4^+, K^+, Mg^{2+}, Ca^{2+}) by ion-exchange chromatography equipped with conductivity detector; (ii) major anions (F^-, Cl^-, NO_3^-, SO_4^{2-}, oxalate (OXL)) by high-pressure ion chromatography equipped with conductivity detector and suppressor; and (iii) selected saccharides, levoglucosan (LVG), mannosan (MAN), galactosan (GAL), arabitol (ARB), mannitol (MNT), and glucose (GLC) by high-pressure ion chromatography equipped with a pulsed amperometric detector. Details are reported in SI section S1. The remaining portions of filters underwent elemental analysis (Al, V, Mn, Fe, Ni, Cu, Zn, As, Cd, Sn, Sb, Pb) by acid digestion (HNO_3–HF–H_2O_2) in a microwave oven followed by ICP-OES and ICP-MS analyses (5300 DV and NexION 350X, PerkinElmer, USA, respectively). Details are provided in SI section S1.

In addition, PM_{10} samples were collected alongside $PM_{2.5}$ according to the EN12341:2014 on QFF (Whatman QMA) and analyzed for particulate mass (UNI EN 12341:2014) and 8 polycyclic aromatic hydrocarbons (benz(a)anthracene (BaA), chrysene (Chry), benzo(b)fluoranthene (BbF), benzo(k)fluoranthene (BkF), benzo(a)pyrene (BaP), indeno(1,2,3-c,d)pyrene (IP), dibenzo(a,h)anthracene (DBahA) and benzo(g,h,i)perylene (BghiP)) following the UNI EN 15549:2008 and UNI CEN/TS 16645:2014 by HPLC interfaced with a multi-wavelength fluorescence detector (2695 series Alliance and 2475, Waters, USA; Masiol et al., 2013). PM_{10}-bound PAH analyses were performed on selected filters and by extracting 2 to 3 filters together. Therefore, the data represents the average concentration over several days. Since PM-bound PAHs are mainly distributed into the submicrometric PM fraction (e.g., Lammel et al., 2011; Zhang et al., 2020), as confirmed by local studies in the mountain areas of Veneto (ARPAV, 2017), it is assumed that the PM_{10}-bound PAHs concentrations can be matched with the chemical-speciated $PM_{2.5}$ data.

The quality of the analytical procedures was checked by blank controls, by evaluating detection limits (DLs), recoveries through reference materials, accuracy, and repeatability. Details in SI Section S1.

2.3. Ancillary variables

NO, NO_2, NO_x (EN 14211:2012), and O_3 (EN 14625:2012) were also measured on an hourly basis at the same station. Weather variables including air temperature (°C), relative humidity (%), pressure (mbar), solar irradiation (W m^{-2}) wind speed (m s^{-1}) and direction were measured at a nearby station (AE) approx. 3.5 km NE of the city center. The water mixing ratio (g kg^{-1}) was computed from the weather data.

The EC-tracer method (Cabada et al., 2004) was preliminarily applied to estimate the primary (POC) and secondary (SOC) organic carbon from OC/EC data. Details are reported in SI section S2. Additional variables were computed from the analytical data as proxies for specific atmospheric and/or aerosol properties; details are provided in SI section 3. Briefly, since hydroxyl radical is not measured, the oxidative potential of the atmosphere is indirectly assessed through the sum of measured atmospheric oxidants (OX= NO_2+O_3 [ppb], Kley et al., 1999). The nitrogen oxidation ratio (NOR) depicts the degree of atmospheric conversion of NO_2 to particulate-phase nitrate (Colbeck and Harrison, 1984). The neutralization ratio (NR, Colbeck and Harrison, 1984; Bencs et al., 2008; Engelhart et al., 2011) describes the degree of neutralization of sulfate and nitrate by ammonium.

The CALMET model was used to estimate the planetary boundary height (Hmix) and atmospheric stability. Details are reported in SI section S4. The estimation of the weather-related impacts on the net energy demand for heating was assessed by computing the heating degree-days (HDD; Thom, 1954; Quayle and Diaz, 1980; Spinoni et al., 2018). Details in SI section S5 and Table S1. Essentially, HDDs are proportional to the amount of energy needed to heat the internal environment in a cold climate to a specified base temperature for a given period (15.5 °C and daily basis in this case; Spinoni et al., 2015). Consequently, the HDD value reflects the potential biomass consumption for domestic heating each day.

2.4. Mass closure

Mass closure was assessed by summing the concentrations of the analyzed chemical species with assumptions to account for elements not directly measured, mostly hydrogen and oxygen in both organic and inorganic compounds. Existing methods are reviewed by Chow et al. (2015). The compositions of major chemical components (organic matter (OM), elemental carbon (EC), sulfate, nitrate, ammonium (SNA), crustal material (CRU), sea-salt aerosol (SSA), and other trace elements and ions (OTHERS)) were assessed (details in SI section S6).

2.5. Source apportionment

$PM_{2.5}$ sources were identified and quantified by USEPA PMF version 5 (Hopke, 2015; Paatero, 1997; Paatero and Tapper, 1994). Data below DLs were set as DL/2, with an uncertainty of 5/6 of the corresponding DL. Uncertainties for data > DLs were carefully assessed by propagating errors from all steps of the adopted analytical procedures, including analytical uncertainties in samples and blanks, recoveries, and sampler performances. Uncertainty for the total variable ($PM_{2.5}$) was set to 300% of the concentration to prevent it from driving the model (Kim et al., 2003). The optimal solution was identified based on the best practice reported in the relevant literature (Belis et al., 2014; Brown et al., 2015; Hopke, 2016; Reff et al., 2007) and the evaluations from the built-in diagnostic tools. Rotational ambiguity was assessed through displacement (DISP); uncertainties were estimated by bootstrap (BS, replicates = 200, Min. correlation, r = 0.6), and the combined BS-DISP (Paatero et al., 2014) was calculated to check the overall stability of the solutions.

The remaining data analyses were computed by R 4.3.3 (R Core Team, 2022). The location of potential local sources was assessed by mapping the average pollutant concentrations by wind speed and direction as a continuous surface in bivariate polar plots (Carslaw and Ropkins, 2012).

2.6. Dispersion normalization

Dispersion normalization using the ventilation coefficient (VC) was used to account for the effects of meteorological variations on air quality and to improve source apportionment results (e.g., Chen et al., 2022; Dai et al., 2020; Sofowote et al., 2021). Essentially, the atmospheric dispersion is assumed to be proportional to the product of wind speed (ws) and boundary layer height:

$$VC_i = ws_i \times Hmix_i \quad (1)$$

where i denotes each measurement period (days). Since ws and Hmix are provided on an hourly basis, the daily averages are used. The daily concentration values are then normalized:

$$C_{VC,i} = C_i \times \frac{VC_i}{\overline{VC}} \quad (2)$$

where $C_{VC,i}$ is the normalized concentration, C_i is the measured concentration for the period i, and $\overline{VC}$ is the average VC over the whole sampling period.

2.7. Detection of persistent inversion periods

Persistent thermal inversions negatively affect air pollution in Alpine valleys. Since vertical temperature profiles are not experimentally

measured, a simple estimation of the inversion strength across the valley was computed using air temperature from nearby weather stations at different elevations. This method was adapted from Largeron and Staquet (2016), who reported persistent inversion in the Grenoble area (French Alps) related to elevated PM_{10} concentrations. This method returns similar results to other methods available in literature such as the heat deficit evaluation (Whiteman et al., 1999).

Hourly weather data from 8 stations (Fig. S1; Table S2) managed by ARPAV were initially investigated. These ground-based stations are located at different elevations (264 m–1603 m ASL) within the Valbelluna or in the surrounding mountains. Since only three stations (FE, SG, AE) are located in the center of the valley floor at 264–379 m a.s.l., these stations were paired with three more stations located at high elevation (MA, MC, FA, at 1415–1603 m a.s.l., respectively). The horizontal homogeneity of air temperature was preliminarily checked by correlating the hourly-resolved weather data measured at low- and high-elevation stations during the study period. Assuming horizontal homogeneity of the air temperature field over the area, the bulk temperature gradient ($\Delta T/\Delta H$) for each pair of stations was computed and used as a proxy of the stability of the boundary layer into the valley. $\Delta T/\Delta H$ represents the ratio between the difference in air temperature to the difference in height between the high- and low-elevation stations:

$$(\Delta T/\Delta H)_{i,k} = \frac{T_{i,k(\text{ high})} - T_{i,k(\text{ low})}}{H_{k(\text{ high})} - H_{k(\text{ low})}} \quad (3)$$

where i denotes each measurement period (hourly data, in this case), k is a station pair [1,3], $H_{k(high)}$ and $H_{k(low)}$ represent the station elevation and $T_{i,k(high)}$ and $T_{i,k(low)}$ represent the air temperature measured at the time i of the pair k at the high and low station respectively. Table S3 summarizes the characteristics of station pairs.

$\Delta T/\Delta H$ is considered a valid indicator of the stability of the boundary layer when an inversion occurs. According to Largeron and Staquet (2016), $\Delta T/\Delta H > 0$ indicates that an inversion is present between the two stations but not necessarily that the entire layer between the two stations is filled by the inversion. Therefore, inversions were identified by evaluating the temporal patterns of daily-averaged $\Delta T/\Delta H$ ratios. Periods with daily $\Delta T/\Delta H > 0$ for more than 3 days were considered persistent temperature inversions.

3. Results and discussion

Fig. 1 shows the distributions of concentrations of $PM_{2.5}$ and analyzed $PM_{2.5}$-bound species; Fig. S2 reports the distributions of meteorological, gaseous pollutant, and other ancillary variables. The averaged concentration of major (>1% wt) analyzed species followed the order (in $\mu g\ m^{-3}$: OC (6.2) > NO_3^- (2.7) > EC (1.9) > LVG (0.9) > NH_4^+ (0.8) > SO_4^{2-} (0.7) > K^+ (0.4) > Al (0.3). The carbonaceous fraction (OC + EC) accounted for 49% of the total $PM_{2.5}$ mass (8.1 $\mu g\ m^{-3}$). EC and OC were strongly correlated (r = 0.93), were generally highly correlated with anions, K^+, ammonium, all organics (including BB tracers but not GLC), Zn and Cd but not well correlated with other cations and elements (Fig. S3).

The average OC/EC ratio was 3.2 (range 2–5) with the higher values recorded in January. An OC to EC ratio for the primary sources $(OC/EC)_p$ of 2.42 was found adopting the EC-tracer method (Fig. S4). POC (average 4.5 $\mu g\ m^{-3}$, 28% of the total $PM_{2.5}$ mass) largely exceeded SOC (1.7 $\mu g\ m^{-3}$, 9%), showing SOC/POC ratios ranging from 0 to 1.1 (average 0.36). Water-soluble inorganic ions (WSIIs) represented the second largest contribution to the total $PM_{2.5}$ mass (26%, 4.6 $\mu g\ m^{-3}$). The major WSII component was the sulfate–nitrate–ammonium (SNA) aerosol forming in the atmosphere following well-established thermodynamic processes involving the H_2SO_4–HNO_3–NH_3 system (Seinfeld and Pandis, 2016). SNA accounted for approx. 22% of the total $PM_{2.5}$ mass (4 $\mu g\ m^{-3}$) and 77% of total WSIIs. Nitrate accounted for 16% of $PM_{2.5}$ mass indicating that ammonium nitrate is the dominant form of the secondary inorganic aerosol (SIA) as commonly reported in Northeastern Italy (Masiol et al., 2015). Generally, all ions were moderately to strongly correlated to each other, except Mg^{2+} and Ca^{2+} (Fig. S3). They are also well correlated with organic tracers except GLC.

Among the common BB tracers (Bhattarai et al., 2019; Puxbaum et al., 2007; Schkolink et al., 2006; Simoneit, 2002), LVG exhibited higher average concentrations followed by K^+, MAN, and GAL (Fig. 1). Very high correlations were found among the BB tracers (Figures S3 and S5a-c), with coefficients of determination ranging from 0.94 (K^+-LVG) to 0.98 (LVG-MAN, MAN-GAL). LVG also exhibited a strong linear relationship ($r^2 = 0.88$) with POC but a much lower ($r^2 = 0.58$) with SOC (Figs. S5d and e), clearly reflecting the primary nature of this specific marker.

GLC, MNT and ARB are often used as tracers for primary biogenic organic aerosol (Marynowski and Simoneit, 2022; Pashynska et al., 2002; Samaké et al., 2019; Yttri et al., 2007). Specifically, GLC is associated with plant materials (e.g., pollen, fragments of leaves) or soil emissions, while MNT and ARB are generally associated with airborne fungal spores (e.g., Rathnayake et al., 2017; Samaké et al., 2019; Wan et al., 2019). Strong positive and significant relationships (Figs. S3 and S6) were found between MNT and ARB (r = 0.83) and between polyols (defined as MNT + ARB) and OC (r = 0.88), while no correlation was found between GLC and polyols. The concentrations of GLC, MNT and ARB are in the range of those collected at different locations and seasons, as reviewed by Golly et al. (2019).

OXL, a derivative form of oxalic acid, is generally associated with secondary formation processes, representing an end-product of the oxidation of organic gas-phase species (Ervens et al., 2004). The concentration varied between 28 and 253 ng m^{-3} (average 96 ng m^{-3}), similar to concentrations measured at an alpine remote site in France (95.5 ng m^{-3} during all seasons; Golly et al., 2019) but lower than those measured in urban areas in Northern Italy, (Milan 122 ng m^{-3} in winter; Perrone et al., 2012). OXL accounted for 0.7–4.9% of total OC (average 1.8%) and was strongly positively correlated with SNA ions ($0.81 < r < 0.88$; Fig. S3), stressing its main secondary origin. However, it is not strongly correlated with POC (r = 0.44) or SOC (r = 0.55) from the EC-tracer method. Ratios between specific chemical species are often used as proxies for inferring sources and processes and are discussed in Section S7 and Figs. S7 and S8.

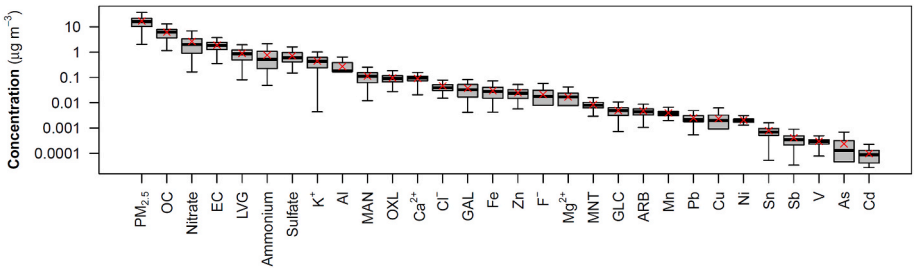

Fig. 1. Boxplots of the analyzed compounds and elements in $PM_{2.5}$ at BL. For each species, the boxplots show: line = median, box = inter-quartile range, whiskers = ±1.5*inter-quartile range; red cross = arithmetic means; outliers and extremes are not shown.

3.1. Nitrate aerosol formation

Insights into the nitrate aerosol formation arise from some simple steps and a few assumptions. Ammonium sulfate is preferentially and irreversibly formed when sulfuric acid and ammonia are available, taking priority over ammonium nitrate because of its low vapor pressure. Under ammonium-rich conditions (NH_4^+/SO_4^{2-} molar ratio >2), it can be assumed that ammonium sulfate is the preferred form of sulfate, otherwise ammonium sulfate and bisulfate may form in ammonium-poor conditions, increasing the aerosol acidity. The reconstruction of the ammonium concentration from nitrate and sulfate indicated a quite good fit ($r^2 \geq 0.95$; Fig. S9a), with slopes close to unity but positive intercepts. However, ammonium-deficient conditions were generally observed (points over the 1:1 line). This ammonium imbalance was also responsible for the neutralization ratios below unity (Fig. S2), as previously reported in Belluno (Masiol et al., 2015). Despite this, the cation-to-anion ratio in charge equivalents exhibits a perfect ion balance (slope 0.996, $r^2 = 0.97$; Fig. S9b) even if Na^+ was not included (below DL). This result is possibly explained by the formation of mixed salts.

As a simple way to better elucidate the factors affecting ammonium nitrate formation, the linear regression between the NH_4^+/SO_4^{2-} and NO_3^-/SO_4^{2-} molar ratios for ammonium-rich conditions ($r^2 = 0.69$; Fig. S9c) returns an intercept of 1.14 and a slope of 0.79, which ratio (1.44) below 2 further supports the assumption that part of the sulfate existed in other forms, such as ammonium bisulfate (Pathak et al., 2009) or mixed salts. After the sulfate aerosol formed, ammonium nitrate forms when more ammonium is available, i.e., when the excess-NH_4^+ > 0 (details in SI section S3). Fig. 2 shows that the excess-NH_4^+ ranges from −4 to 233 nmol m^{-3} (average 32 nmol m^{-3}) with 77% of samples under ammonium-rich regimes. Despite the uncertainty of the adopted method (which does not consider the gas-phase acids and ammonia and analytical uncertainties), possible sampling artifacts (limited by the low air temperatures and strict sampling protocols) and the large variability of data, the nitrate to excess-NH_4^+ ratios are mostly over the 1:1 line, again indicating the possible formation of mixed nitrate salts.

3.2. Mass closure

In this study, the primary (POM) and secondary (SOM) organic matter were separately estimated from the POC and SOC from the EC-tracer method, considering the different oxidation between the primary and secondary organic aerosol. A 1.2 factor was applied to POC, assuming the composition of fresh aerosol in urban areas (Chow et al., 2002), while SOC was multiplied by 1.8, a value indicative of aerosol from BB emissions after ageing for ~3 days from smog chamber studies (Lim et al., 2019). These values agree with the 1.6 value used in previous studies in BL for total OC (Masiol et al., 2020). Crustal material and salt were computed according to equations in Hand (2011). Secondary inorganic aerosol was simply assessed as SNA.

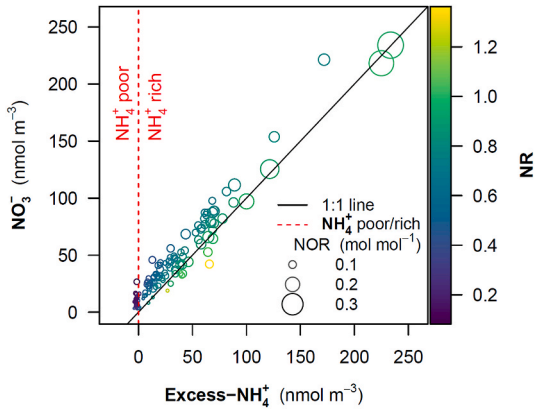

Fig. 2. Scatter plots of nitrate vs. excess-ammonium (in molar concentrations). The plot also shows other variables computed in the study (details in SI section S2): the vertical red line shows the split between ammonium-poor and -rich conditions; the dimension of points is proportional to the nitrogen oxidation ratio (NOR); the color of points shows the neutralization ratio (NR). (For interpretation of the references to color in this figure legend, the reader is referred to the web version of this article.)

Results (Fig. 3a) show good mass reconstruction (slope = 0.96) and fit ($r^2 = 0.94$, RMSE 2.2 μg m^{-3}) with concentrations of the various $PM_{2.5}$ chemical components over the whole sampling period following the order (in μg m^{-3}): POM (5.5) > SNA (4.2), crustal material (3.4) > SOM (3.1) > EC (1.9) > other species (0.5) > sea-salt (0.1) (Fig. 3b). The relative contributions of the major chemical components were quite constant during the sampling period (Fig. S10), but the absolute concentrations of POM, SOM, SIA, EC, and other species significantly increased from October to January (Fig. 3c), as indicated by the Kruskal-Wallis test ($p < 0.05$) and its pairwise comparisons using Dunn's post-hoc test ($p < 0.0002$). No other differences were statistically significant.

3.3. Source apportionment

Variables were screened for their information content (Paatero and Hopke, 2003): a total of 26 variables were inputted as "strong", while 3 variables with signal-to-noise ≤1 (Al, Cu, As) were set as "weak" thereby tripling their uncertainties. Four days were excluded from the analysis: 12 October because significantly worsened the diagnostics and exhibited high-scaled residuals for multiple species, probably due to construction activities or contamination, and 5–7 December because concentrations of $PM_{2.5}$ and multiple species were below DLs due to intense precipitation. Solutions were explored from 3 to 7 factors. The most physically plausible results were obtained with a 5-factor solution, for which the minimum Q values were evaluated over 200 runs. The selected solution also exhibited the Q_{true} value closest to the theoretical (Q_{exp}) value ($Q_{true}/Q_{exp} \approx 0.97$) and optimal diagnostics: (i) all runs converged; (ii) all species had stable Q values over 200 runs; (iii) the absolute scaled residuals were symmetrically distributed and the number of values exceeding ±3 was minimized; (iv) modeled total variable ($PM_{2.5}$) was successfully predicted ($r^2 = 0.97$); (v) no swaps by factor were found in DISP with $\%dQ = 0$; and (vi) swaps in BS were minimized (<10%) with no unmapped factors. The G-space showed no edges (Paatero et al., 2005), thus FPEAK solutions were not investigated. No constraints (Brown et al., 2015) were applied after extensive exploration showed no improvement in the profiles. According to previous literature (Zíková et al., 2016), the min-max ranges calculated by DISP under the constraint that the difference (dQ = base-modified) is no greater than the $dQ_{max} = 4$ were used to assess the boundaries of source profiles.

Results were interpreted based on the presence of known tracers in the source profiles (Fig. 4), the ratios of selected chemical species in the profiles (Fig. 5), the local directionality of factors shown by polar plot analysis (Fig. S11), the temporal patterns of contributions throughout the sampling period (Fig. S12), and the correlations with PAHs, weather and ancillary variables (Fig. S13).

3.3.1. Secondary aerosol

Factor 1 presents a high share of ammonium (74% of specie sum), nitrate (46%), sulfate (37%) and OC (11%), but also contains significant fractions of OXL and As. It strongly correlates ($r > 0.65$) with PM_{10} and moderately correlates ($0.45 < r < 0.65$) with most PAH congeners (Fig. S13). This source represents secondary aerosols mostly composed of ammonium nitrate, ammonium sulfate/bisulfate and organics. The nitrate-sulfate-ammonium association remains unchanged by increasing the number of factors. Generally, the chemistry of secondary nitrate competes with secondary sulfate, but the presence of a cumulative source is not surprising in this study. Secondary nitrate is highly favored by cold temperatures (period average: 4.3 °C) and high relative humidity (period average: 90%) (Seinfeld and Pandis, 2016) usually

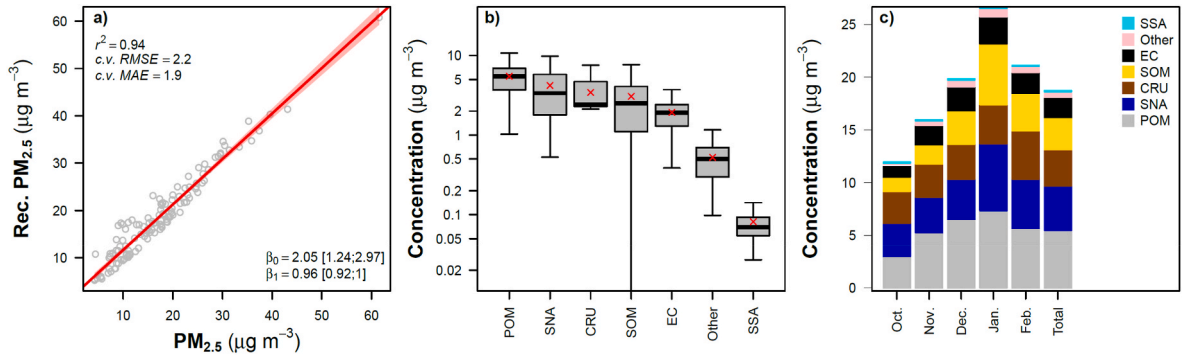

Fig. 3. Results of the mass closure: a) linear regression showing the fit between the measured and reconstructed $PM_{2.5}$ masses; b) the distributions of the 7 major $PM_{2.5}$ components (details in SI section S6); c) cumulative concentrations of the 7 major $PM_{2.5}$ components reconstructed by the mass closure (sorted by increasing average contributions over the whole sampling period). (For interpretation of the references to color in this figure legend, the reader is referred to the web version of this article.)

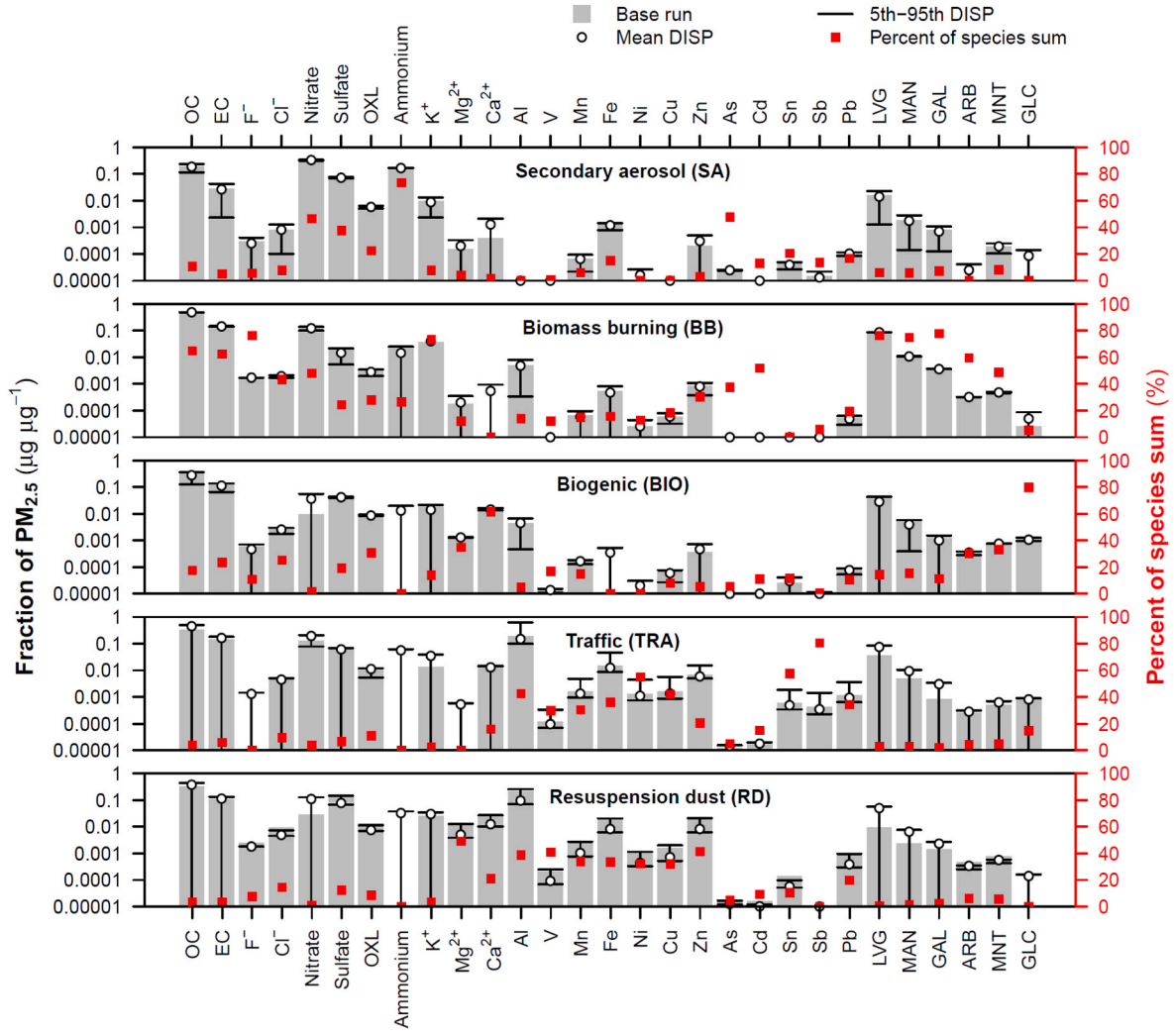

Fig. 4. PMF factor profiles. Left y-axis: bars represent mass contribution of the base run; open circles represent the mean DISP values with the error bars providing the range (minima and maxima values) of DISP values. Right y-axis: red filled squares show factor contributions in percent of species sum. (For interpretation of the references to color in this figure legend, the reader is referred to the web version of this article.)

recorded in the study area in winter and transition seasons.

Conversely, sulfate production, despite being more thermodynamically stable, is enhanced by photochemistry and is mostly dominating during warm seasons (Squizzato et al., 2013). The presence of a relatively large fraction of OC reflects the production of secondary organic aerosol (SOA) enhanced in the presence of pre-existing acidic particles (Deng et al., 2021; Hallquist et al., 2009; Kuwata et al., 2015; Shrivastava et al., 2017), resulting in internally mixed aerosols. This factor has the highest OC/EC ratio (Fig. 5), approximately 3-folds higher than the primary OC/EC computed with the EC-tracer method. This result

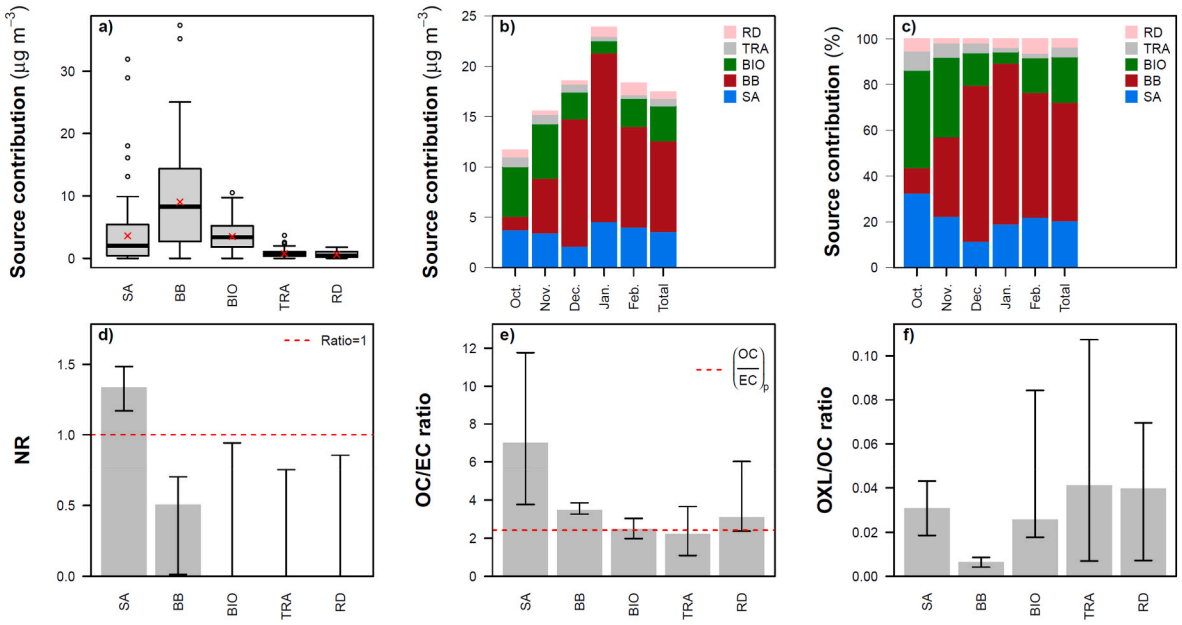

Fig. 5. PMF results: a) boxplots of the source contributions; b) stacked bar plot showing the average source contributions of the 5 sources by months and over the whole sampling period; c) relative contribution of the 5 sources by months and over the whole sampling period; d), e), and f) ratios among chemical species in the PMF profiles (the grey bars refer to the concentration in the base run; error bars show the uncertainty of the ratios as 5-95th percentile ranges over the 200 BS runs). (For interpretation of the references to color in this figure legend, the reader is referred to the web version of this article.)

indicates the uptake of SOA on primary particles. The 22% of total OXL in this factor stresses its secondary nature (Zhou et al., 2015). OXL is principally generated in the atmosphere via atmospheric oxidation of higher homologues of long-chain diacids as well as from other pollution-derived organic precursors in gas, heterogeneous, and aqueous phases (Kawamura and Bikkina, 2016; Yang et al., 2022) and was found internally mixed with aged BB particles (Zhang et al., 2017). The relatively high shares of As, Sn and Fe are unusual for a secondary factor. However, the factor does not present swaps with any other factors and the association does not split until a 7-factor solution was investigated, returning poorer diagnostics. Thus, it is unlikely that this chemical association represents distinct sources due to a poorly resolved solution.

The secondary aerosol source accounts for 21% (DISP min-max range 19–29%) of total $PM_{2.5}$ mass (Fig. 5). Polar plot analysis does not show a clear directionality but high concentrations by moderate winds blowing from ENE and S (Fig. S11). The time series shows no clear patterns but the alternation of periods with low and high concentrations. During 21–23 October, a severe SA peak occurred with concentrations up to 32 µg m^{-3} (Fig. S12), i.e., 7-fold higher than the remaining study period.

3.3.2. *Biomass burning*

Factor 2 is responsible for more than half (52%) of total $PM_{2.5}$ mass (Fig. 5) and shows very high shares of traditional BB tracers: anhydrosugars (75–78%), K^+ (73%) as well as high contributions of OC (65%) and EC (62%). It was interpreted as BB emissions mostly composed of mixing of organics, soot and potassium, according to the literature (Lee et al., 2016). The factor concentration constantly increases from October to January (Fig. 5) following HDD ($r = 0.69$) and inversely to air temperature ($r = -0.69$) (Fig. S13). Although this source represents combustion sources likely dominated by residential wood combustion (RWC) (Vicente and Alves, 2018), the possible contribution of open crop residue fires cannot be neglected in autumn. Crop residue burning is not allowed but is still utilized in the post-harvest season. RWC is a known major aerosol source in Europe (Cincinelli et al., 2019; Kukkonen et al., 2020; Yttri et al., 2019). The BB factor is also strongly associated with NO_x and PAHs ($0.68 < r < 0.92$), stressing its primary origin from combustion. A stepwise multiple linear regression was performed between PMF sources (independent variables) and the sum of 8 analyzed congeners (dependent variable). BB was the only independent variable statistically significant ($p < 0.05$). Adopting the Akaike information criterion as an estimator of prediction errors (in both directions), the best model was found with only BB, indicating that almost all PAHs are emitted by this source.

BB does not present clear directionality (Fig. S11) but showed increased concentrations during low wind regimes and moderate easterly winds, compatible with a local origin. The OC/EC ratio of the source profile (BS range 3.3–3.9) is slightly higher than the primary OC/EC ratio found with the EC-tracer method but generally agreed with data reported in literature for emissions of woodstoves burning wooden logs (mainly pine) (2.8 ± 1.3; Zhang et al., 2013) or spruce wood logs (1.2–11.5; Orasche et al., 2012), and pellet stoves burning wood pellet (0.9–4.2; Vicente et al., 2015).

The BB factor also exhibits a moderate share of OXL (28%). Sources of oxalate include primary and secondary emissions from biogenic and anthropogenic sources, such as BB (Kundu et al., 2010). For example, Xu et al. (2020a) showed similar results (BB contributed 25% of OXL during a typical biomass burning period using single particle source analysis). Beyond the primary emission, a possible ageing of BB emissions cannot be excluded from this factor. Recent literature reports that organic aerosol from BB may undergo fast chemical ageing even under wintertime periods with low photochemical activity or nighttime (e.g., Kodros et al., 2020; Yazdani et al., 2023). In addition, the high relative humidity (period average 90% RH, with 34% of sampling days with daily average > 95% RH) may favor the formation of secondary organic aerosols in the aqueous phase (Gilardoni et al., 2016).

The BB factor is also associated with high fractions of fluoride (76%), chloride (43%), and nitrate (48%), which are known to be emitted by BB processes (Calvo et al., 2015; Fine et al., 2001; Jayarathne et al., 2014; Song and Liu, 2023; Vicente and Alves, 2018). Also, it shows high fractions of ARB (59%) and MNT (49%). Despite being typical markers of primary biological aerosols (Marynowski and Simoneit, 2022; Samaké et al., 2019; Xu et al., 2020b), these sugar alcohols are also found in association with primary BB emissions in wintertime (Xu et al., 2019). Moderate shares of Fe, Zn and Cu are not surprising since Schmidl et al. (2008) reported that these elements are emitted by wood stove

combustion of common woods grown in Alpine regions.

3.3.3. Biogenic aerosol

The third factor accounts for 20% of $PM_{2.5}$ mass and is mostly composed of OC. It also exhibits high fractions of EC, GLC, Ca^{2+}, Mg^{2+}, ARB, MNT, and OXL. Although LVG, K^+ and nitrate show moderate base run contributions, their wide DISP intervals toward null contribution indicate that these species have limited associations with this factor. Instead, the presence of GLC, MNT and ARB suggests biogenic emissions. This interpretation is also supported by the decreasing monthly contributions from October to January. The factor also shows a moderate share of elemental carbon but the DISP interval takes EC down to ~66 ng m^{-3}, which is quite a low concentration. Also, the biogenic factor is likely an indicator of SOA from biogenic volatile organic compounds (BVOCs). These BVOCs need a place to condense, and elemental carbon particles will serve as a preferred surface on which to condense because of their unique chain aggregate shape (high surface to volume). Possible secondary origin is also supported by the high shares of OXL and sulfate, indicating possible atmospheric aging. This way, the EC share may be explained by mixing with other material during resuspension or co-emission along with BB source in stoves during cold-start phases. Polar plots analysis (Fig. S11) does not show clear directionality but higher concentrations during moderate to high wind days, which is compatible with the resuspension of material of biological origin from the surrounding forests and green areas.

3.3.4. Traffic and resuspension dust

The last two factors account for a small fraction of $PM_{2.5}$ mass (4% and 3%, respectively; Fig. 5) showing constant monthly contributions and similar profiles. They exhibit significant fractions of Al, transition, and post-transition metals (V, Mn, Fe, Ni, Cu, Zn, Sn and Pb). On the contrary, OC, EC, ammonium, potassium, BB tracers and GLC show wide DISP ranges and are not likely associated with these factors. Metals can be emitted from multiple sources, such as exhaust-related sources (engine corrosion, fuel and lubricant combustion, catalytic converters, particulate filters) as well as from non-exhaust sources (tire and brake wear, muffler ablation) (Amato, 2018; Fussell et al., 2022; Pant and Harrison, 2013). The main differences between the two sources are the presence of high Sn and Sb concentrations in factor 4 and high shares of Ca^{2+} and Mg^{2+} in factor 5. Considering the DISP ranges, nitrate has a moderate value in factor 4, while chloride and fluoride are in factor 5.

Insights upon their interpretation come from wind analysis. Factor 4 shows no directionality and higher concentrations for low-moderate winds, suggesting a source widespread over the city. Traffic is the most likely source. This interpretation is also supported by the similarity with the factor profile for traffic reported in major cities in Veneto (Masiol et al., 2020) considering the specific elements. Factor 5 increased during high wind regimes (correlation with wind speed $r = 0.40$) suggesting dust resuspension. This interpretation is supported by the higher shares of crustal elements (Ca^{2+}, Mg^{2+}) linked to calcareous soils, dolomite and limestones present in the study area, and shares of chlorine, compatible with road salts used as anti-icing and the higher share of Zn, generally associated with tire wear.

3.4. The role of specific sources on the exceedance of European standards

The average $PM_{2.5}$ concentration was 17 μg m^{-3} with 22 days exceeding a daily concentration of 25 μg m^{-3}. The PMF source contributions when the forthcoming daily limit is met vs. exceedances show statistically significant differences only for SA and BB (nonparametric Wilcoxon signed rank test) at $p < 0.01$ (Fig. S14a). Average increases of 7.6 μg m^{-3} of SA and 9.9 μg m^{-3} of BB were recorded during exceedances with respect to days with daily limit value met (Figs. S14b and c).

Thus, these sources must be the main target of air pollution mitigation strategies. By contrast, TRA and RD are not significantly different possibly because current strategies for the mitigation of air pollution (traffic restrictions based upon EURO vehicle's emissions standard) are in force. Thus, specific air pollution mitigation policies for $PM_{2.5}$ should be mostly implemented or strengthened to meet newly proposed limit values during the cold season, targeting the emissions from domestic appliances burning wood.

Wilcoxon sign-rank tests indicated that the $PM_{2.5}$ mass concentration and the contributions of secondary aerosol and BB were statistically significantly ($p < 0.01$) higher in days with ammonium-rich with respect to ammonium-poor conditions. No significant differences were found for other sources. In addition, all days with $PM_{2.5}$>25 μg m^{-3} occurred during ammonium-rich conditions. Thus, the ammonia availability plays a key role over the nitrate aerosol formation and aerosol mass. Since EIs for 2019 in Valbelluna municipalities (INEMAR, 2022) estimate that 90% of ammonia (762 Mg y^{-1}) is emitted by agriculture, of which 90% (688 Mg y^{-1}) come from manure management regarding nitrogen compounds. Therefore, it is necessary that further actions are also implemented at a regional and supra-regional level to reduce ammonia emissions for minimizing the secondary nitrate aerosol.

3.5. The effects of atmospheric dispersion

Generally, the dispersion normalization concentrations of $PM_{2.5}$ were lower than un-normalized data (Fig. S15a), mostly due to the inverse relationship between Hmix (decreasing from October to February) and $PM_{2.5}$ concentration (increasing). A period of high wind regimes (11–14 February) led to very high VC-normalized values at the end of the sampling period. Another high-wind period occurred on 5–7 December along with strong precipitation, but these samples were removed from PMF due to concentrations below DLs. $PM_{2.5}$ concentrations accounting for the VC show a different monthly pattern (Fig. 6 and S15b,c), with higher $PM_{2.5}$ concentrations in October and February (only 14 days are available in February). These differences were statistically significant (nonparametric Wilcoxon signed rank test) during all periods, except in February (Fig. 6).

Examining the single sources, BB shows the main differences, with significantly lower VC-normalized concentrations in November–January. Also, BIO and RD showed statistically significant differences between raw and VC-normalized contributions with higher concentrations in October and lower in November–December. This result stresses again the relationship of BIO and RD, being generated by the resuspension of natural and anthropogenic materials, respectively. TRA shows lower VC-normalized concentrations in November and December, while SA only in January. In summary, the dispersion normalization results show that the BB source is more affected by the VC factor because the ventilation conditions of the valley favor the increase in concentrations (normalized VC lower than those detected experimentally). The two resuspension sources are also influenced by atmospheric dispersion, but the October concentrations are effectively dispersed, probably because the higher average daily height of the planetary boundary layer.

3.6. The effects of persistent inversions

A preliminary evaluation of the air temperature shows a strong correlation ($0.68 < r < 0.99$) among the 8 selected weather stations (Fig. S16) with the higher values found between the 3 low-elevation (FE, SG, AE, TO; $0.96 \leq r \leq 0.99$) and the 3 high-elevation (MA, MC, FA; $0.94 \leq r \leq 0.99$) stations. The linear relationships of air temperatures confirm this strong correlation (Figs. S17a–c). By contrast, the linear relationships between pairs of high-elevation and low-elevation stations (Figs. S17d–e) show temperature differences between the valley and the mountaintop are much less correlated and exhibit a clear edge that closely follows the dry adiabatic lapse rate (DALR, 9.8 °C km^{-1}). These latter scatterplots also show that most of the observations lie between the DALR and the 1:1 isothermal line. However, a limited number of points lie below the isothermal, i.e., the high elevation station recorded higher temperature values than the low elevation.

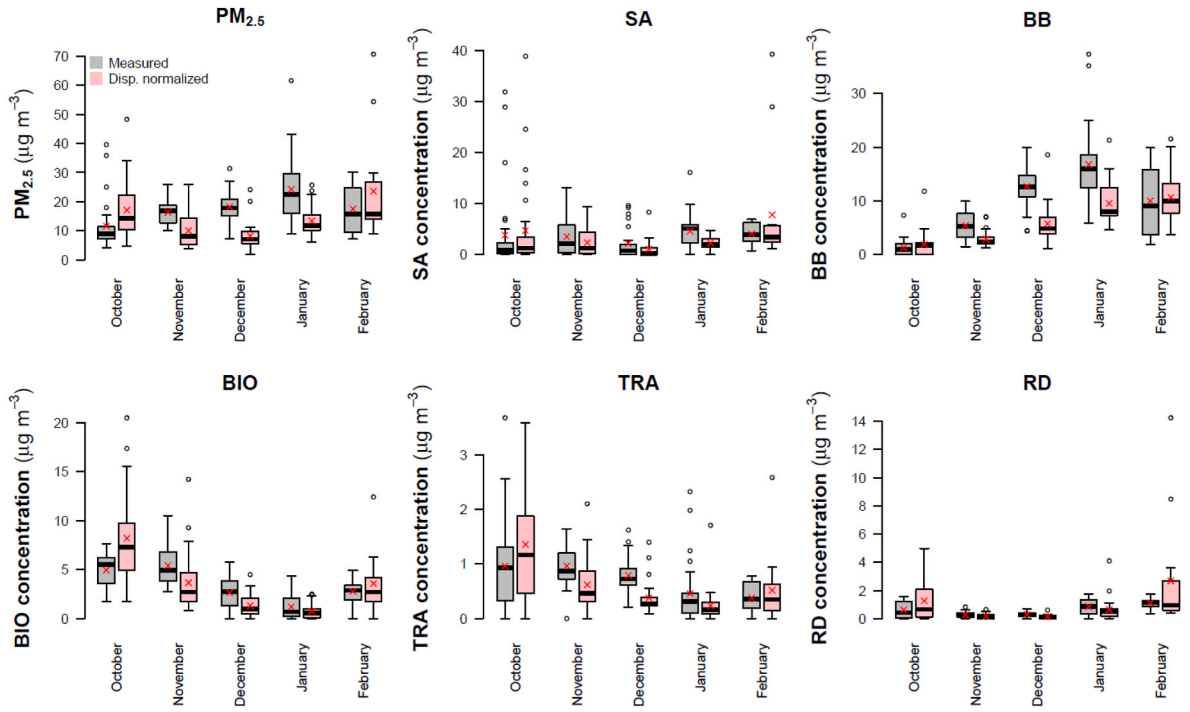

Fig. 6. $PM_{2.5}$ and PMF source contributions: measured $PM_{2.5}$ and contribution modelized by PMF are in grey; dispersion-normalized concentration in pink (For interpretation of the references to color in this figure legend, the reader is referred to the web version of this article.).

The time series at hourly and daily resolutions (Fig. S18) also show generally lower temperatures in the high-elevation stations, but also periods with potential thermal inversions. Similar results were reported by Largeron and Staquet (2016) in the Grenoble Valley, France, emphasizing that local processes do not strongly account for the spatiotemporal variability of air temperature inside the valley and that synoptic scale fluctuations may play a major role, especially close to the summits. Thus, horizontal gradients in air temperature are negligible with respect to the vertical changes. This approximation allows considering air temperature horizontally homogeneous across the Valley, being the low-elevation stations AE and FE spaced by 32 km and the high-elevation stations FA and VP spaced by 43 km.

Based on the horizontal homogeneity assumption for the air temperature at the low- and high-elevation stations, 3 pairs of weather stations were selected to be representative of the $\Delta T/\Delta H$ ratios over all the valley (FA-AE for the NE valley, MC-SG for the center, and MA-FE for SW; characteristics of station pairs are summarized in Table S3) and the temperature gradient ($\Delta T/\Delta H$) for each pair of stations was computed. The $\Delta T/\Delta H$ at different station pairs were strongly correlated (Fig. S19) between pairs of stations, indicating that potential inversions filled the whole valley.

Fig. 7a and b shows the hourly and daily $\Delta T/\Delta H$, respectively. Six

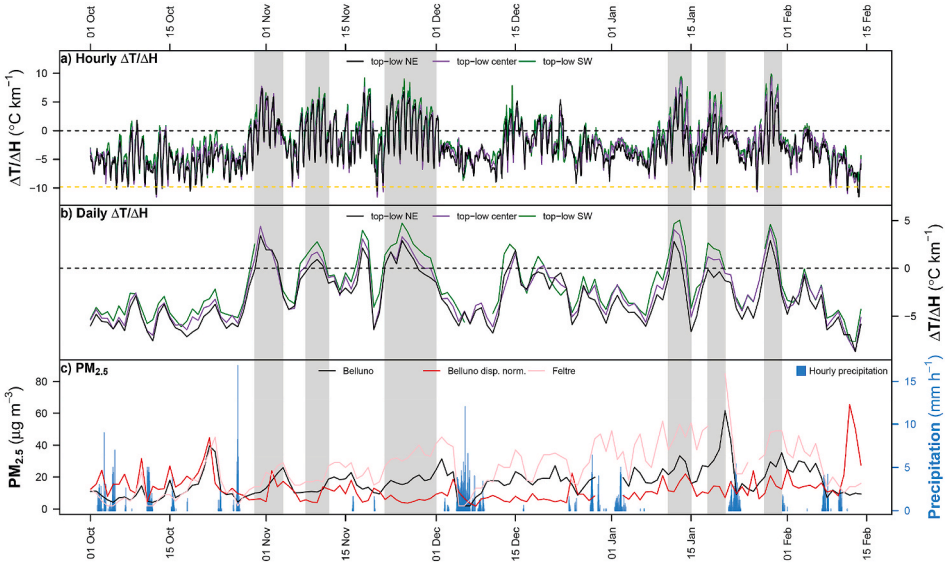

Fig. 7. Identification of the persistent thermal inversion periods: a) hourly-resolved $\Delta T/\Delta H$, b) daily averaged $\Delta T/\Delta H$, and c) concentrations of PM2.5 measured at Belluno (raw data in black, VC-normalized in red) and in Feltre. (For interpretation of the references to color in this figure legend, the reader is referred to the web version of this article.)

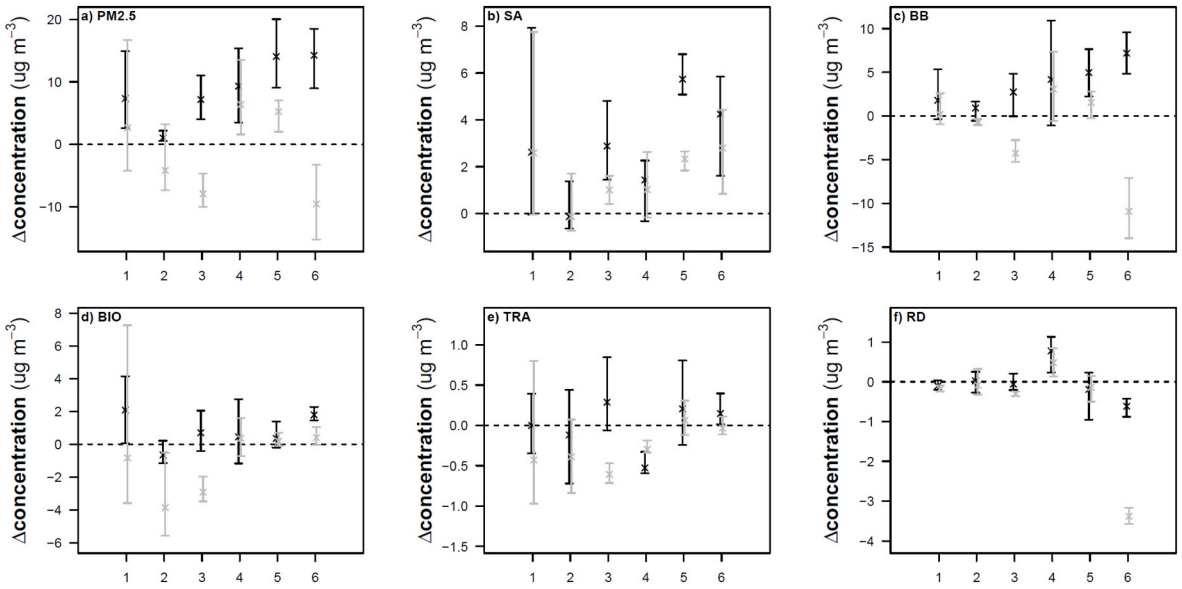

Fig. 8. Differences between the average (points) min and max (bars) $PM_{2.5}$ and PMF source contributions measured during the persistent inversion periods and the concentrations measured 2 days before. Raw data are shown in black; VC-normalized concentrations in grey.

periods with daily $\Delta T/\Delta H > 0$ for more than 3 days were considered persistent temperature inversions (Table S4). Generally, these periods were characterized by or just followed high atmospheric pressure days (Fig. S12), whose effect was compatible with the instauration of inversion conditions in valleys. The $PM_{2.5}$ concentration and the PMF source contributions during the 6 inversion periods are then compared with the concentrations measured two days before. Results indicate a general increase in air pollution during the inversion (Fig. 8). $PM_{2.5}$ concentrations were higher in all inversion periods (0–20 μg m^{-3}) as well as SA (0–8 μg m^{-3}) and BB (0–10 μg m^{-3}). The remaining sources did not show clear patterns. Fig. 8 also shows the VC-normalized concentrations, whose effects on air pollution were less evident, indicating that the dispersion normalization is also able to account for the effects of thermal inversions in valleys.

4. Conclusions

This study identifies the main sources of $PM_{2.5}$ in a major city located within an Alpine valley and quantifies the potential effects of atmospheric dispersion and persistent temperature dynamics. The results show that biomass combustion (52%) and the secondary aerosol fraction (21%) mostly contribute to the $PM_{2.5}$ mass concentration. These sources are responsible for excessive $PM_{2.5}$ concentrations, i.e., they contribute in an even more significant way when considering periods of heavy pollution, here identified as days with $PM_{2.5}$ concentrations higher than 25 μg m^{-3}, which corresponds to the new daily AQS proposed to the European Commission. Other sources include biogenic materials (20%), traffic (4%), and resuspension dust (3%).

Although limited by the uncertainty of the mixing layer height modeling, complex landscape and wind dynamics in mountain environments, the calculation of concentrations normalized by the ventilation coefficient suggests that biomass burning is significantly affected by local atmospheric dispersion. Also, biomass burning and secondary aerosol increase significantly during periods in which a thermal inversion is persistently established in the valley, conditions that likely occur in winter. This result is particularly worrying since mountain valleys are frequently prone to long-lasting inversion conditions, mostly occurring overnight and during cold seasons, or in periods with weak synoptic forcing.

Under this view, considering the effects of local meteorology, the new standard for air quality planned for 2030 will be difficult to achieve without strong intervention and the implementation of successful mitigation strategies at a local scale aiming to successfully reduce the local emissions from space heating, mostly from wood burning. Thus, to attain the coming EU standards, a major effort will be needed to switch home heating to cleaner fuels or improve the combustion efficiency of wood stoves and boilers. These recommendations are not inconsistent with climate policies encouraging biomass as a climate-neutral (non-fossil) fuel but suggest revising and integrating the EU policies to mitigate the potential adverse effects on air quality. In addition, emissions of secondary aerosol precursors must also be lowered but on an interregional scale encompassing the Alpine area. In particular, non-attainments occur during ammonium-rich conditions. Thus, particular care should be given to the control of ammonia emissions.

Beyond the local importance of these results for attaining forthcoming European AQ standards, this study demonstrated that the combination of a traditional source apportionment approach with simple data analysis on weather parameters is useful to quantitatively account for the effects of atmospheric dispersion potential and persistent thermal inversions in an Alpine valley.

CRediT authorship contribution statement

Mauro Masiol: Writing – review & editing, Writing – original draft, Validation, Methodology, Investigation, Funding acquisition, Formal analysis, Data curation, Conceptualization. **Gianni Formenton:** Writing – review & editing, Writing – original draft, Validation, Resources, Methodology, Investigation, Formal analysis, Conceptualization. **Flavia Visin:** Validation, Methodology, Formal analysis. **Alessandro Bonetto:** Validation, Methodology, Formal analysis. **Manuela Rovea:** Validation, Methodology, Formal analysis. **Silvia Ficotto:** Validation, Methodology, Formal analysis. **Elisa Danesin:** Validation, Methodology, Formal analysis. **Tommaso Toffanin:** Validation, Methodology, Formal analysis. **Anita Maggiulli:** Validation, Methodology, Formal analysis. **Maria Battistel:** Writing – review & editing, Validation, Methodology, Formal analysis. **Giovanna Mazzi:** Writing – review & editing, Validation, Methodology, Formal analysis. **Matteo Feltracco:** Writing – review & editing, Validation, Methodology, Formal analysis. **Andrea Gambaro:** Writing – review & editing, Project administration, Funding acquisition, Conceptualization. **Philip K. Hopke:** Writing – review & editing, Writing – original draft, Methodology, Investigation, Conceptualization.

Declaration of competing interest

The authors declare that they have no known competing financial interests or personal relationships that could have appeared to influence the work reported in this paper.

Data availability

Data will be made available on request.

Acknowledgements

This study was funded by the European Union - *NextGenerationEU*, in the framework of the iNEST - *Interconnected Nord-Est Innovation Ecosystem* (iNEST ECS_00000043 – CUP H43C22000540006). The views and opinions expressed are solely those of the authors and do not necessarily reflect those of the European Union, nor can the European Union be held responsible for them. Also, the views and conclusions expressed in this paper may not reflect those of ARPAV. Authors also thankfully acknowledge Dr. Maria Sansone and ARPAV Centro Meteorologico di Teolo for weather data from stations and CALMET; the European Environment Agency for providing CORINE Land Cover 2012 data. PKH acknowledges the financial support of Ca' Foscari University of Venice visiting scholars' program.

Appendix A. Supplementary data

Supplementary data to this article can be found online at https://doi.org/10.1016/j.atmosenv.2024.120556.

References

Amato, F. (Ed.), 2018. Non-exhaust Emissions: an Urban Air Quality Problem for Public Health; Impact and Mitigation Measures. Academic Press. ISBN: 9780128117705.

ARPAV, 2017. Qualità dell'Aria. Caratterizzazione delle polveri PM10 a Misurina 2016 - 2017. ARPAV. https://www.arpa.veneto.it/arpav/chi-e-arpav/file-e-allegati/dap-belluno/aria/qualita-dellaria-prov-bl/comune-di-auronzo-di-cadore/caratterizzazione-delle-polveri-pm10-a-misurina2016-2017.pdf.

Belis, C., Larsen, B.R., Amato, F., Haddad, I. El, Favez, O., Harrison, R.M., Hopke, P.K., Nava, S., Paatero, P., Prévôt, A., Quass, U., Vecchi, R., Viana, M., 2014. European guide on air pollution source apportionment with receptor models. JRC Ref. Rep 88. https://doi.org/10.2788/9307.

Beloconi, A., Vounatsou, P., 2023. Revised EU and WHO air quality thresholds: where does Europe stand? Atmos. Environ. 314, 120110 https://doi.org/10.1016/j.atmosenv.2023.120110.

Bencs, L., Ravindra, K., De Hoog, J., Rasoazanany, E.O., Deutsch, F., Bleux, N., Berghmans, P., Roekens, E., Krata, A., Van Grieken, R., 2008. Mass and ionic composition of atmospheric fine particles over Belgium and their relation with gaseous air pollutants. J. Environ. Monit. 10, 1148–1157. https://doi.org/10.1039/b805157g.

Bhattarai, H., Saikawa, E., Wan, X., Zhu, H., Ram, K., Gao, S., Kang, S., Zhang, Q., Zhang, Y., Wu, G., Wang, X., Kawamura, K., Fu, P., Cong, Z., 2019. Levoglucosan as a tracer of biomass burning: recent progress and perspectives. Atmos. Res. 220, 20–33. https://doi.org/10.1016/j.atmosres.2019.01.004.

Brown, R.J.C., Beccaceci, S., Butterfield, D.M., Quincey, P.G., Harris, P.M., Maggos, T., Panteliadis, P., John, A., Jedynska, A., Kuhlbusch, T.A.J., Putaud, J.P., Karanasiou, A., 2017. Standardisation of a European measurement method for organic carbon and elemental carbon in ambient air: results of the field trial campaign and the determination of a measurement uncertainty and working range. Environ. Sci. Process. Impacts 19, 1249–1259. https://doi.org/10.1039/c7em00261k.

Brown, S.G., Eberly, S., Paatero, P., Norris, G.A., 2015. Methods for estimating uncertainty in PMF solutions: examples with ambient air and water quality data and guidance on reporting PMF results. Sci. Total Environ. 518–519, 626–635. https://doi.org/10.1016/j.scitotenv.2015.01.022.

Cabada, J.C., Pandis, S.N., Subramanian, R., Robinson, A.L., Polidori, A., Turpin, B., 2004. Estimating the secondary organic aerosol contribution to PM2.5 using the EC tracer method special issue of aerosol science and technology on findings from the fine particulate matter supersites program. Aerosol Sci. Technol. 38, 140–155. https://doi.org/10.1080/02786820390229084.

Calvo, A.I., Martins, V., Nunes, T., Duarte, M., Hillamo, R., Teinilä, K., Pont, V., Castro, A., Fraile, R., Tarelho, L., Alves, C., 2015. Residential wood combustion in two domestic devices: relationship of different parameters throughout the combustion cycle. Atmos. Environ. 116, 72–82. https://doi.org/10.1016/j.atmosenv.2015.06.012.

Cantelli, A., Monti, P., Leuzzi, G., Valerio, G., Pilotti, M., 2017. Numerical simulations of mountain winds in an alpine valley. Wind Struct. An Int. J. 24, 565–578. https://doi.org/10.12989/was.2017.24.6.565.

Carslaw, D.C., Ropkins, K., 2012. Openair-an R package for air quality data analysis. Environ. Model. Software 27, 52–61. https://doi.org/10.1016/j.envsoft.2011.09.008.

Cavalli, F., Viana, M., Yttri, K.E., Genberg, J., Putaud, J.P., 2010. Toward a standardised thermal-optical protocol for measuring atmospheric organic and elemental carbon: the EUSAAR protocol. Atmos. Meas. Tech. 3, 79–89. https://doi.org/10.5194/amt-3-79-2010.

Chazette, P., Couvert, P., Randriamiarisoa, H., Sanak, J., Bonsang, B., Moral, P., Berthier, S., Salanave, S., Toussaint, F., 2005. Three-dimensional survey of pollution during winter in French Alps valleys. Atmos. Environ. 39, 1035–1047. https://doi.org/10.1016/j.atmosenv.2004.10.014.

Chen, Y., Masiol, M., Squizzato, S., Chalupa, D.C., Zíková, N., Pokorná, P., Rich, D.Q., Hopke, P.K., 2022. Long-term trends of ultrafine and fine particle number concentrations in New York State: apportioning between emissions and dispersion. Environ. Pollut. 310 https://doi.org/10.1016/j.envpol.2022.119797.

Chow, J.C., Lowenthal, D.H., Chen, L.W.A., Wang, X., Watson, J.G., 2015. Mass reconstruction methods for PM2.5: a review. Air Qual. Atmos. Heal. 8, 243–263. https://doi.org/10.1007/s11869-015-0338-3.

Chow, J.C., Watson, J.G., Edgerton, S.A., Vega, E., 2002. Chemical composition of PM2.5 and PM10 in Mexico City during winter 1997. Sci. Total Environ. 287, 177–201. https://doi.org/10.1016/S0048-9697(01)00982-2.

Cincinelli, A., Guerranti, C., Martellini, T., Scodellini, R., 2019. Residential wood combustion and its impact on urban air quality in Europe. Curr. Opin. Environ. Sci. Heal. 8, 10–14. https://doi.org/10.1016/j.coesh.2018.12.007.

Colbeck, I., Harrison, R.M., 1984. Ozone-secondary aerosol-visibility relationships in north-West England. Sci. Total Environ. 34, 87–100. https://doi.org/10.1016/0048-9697(84)90043-3.

Dai, Q., Liu, B., Bi, X., Wu, J., Liang, D., Zhang, Y., Feng, Y., Hopke, P.K., 2020. Dispersion normalized PMF provides insights into the significant changes in source contributions to PM2.5 after the CoviD-19 outbreak. Environ. Sci. Technol. 54, 9917–9927. https://doi.org/10.1021/acs.est.0c02776.

Deng, Y., Inomata, S., Sato, K., Ramasamy, S., Morino, Y., Enami, S., Tanimoto, H., 2021. Temperature and acidity dependence of secondary organic aerosol formation from ?-pinene ozonolysis with a compact chamber system. Atmos. Chem. Phys. 21, 5983–6003. https://doi.org/10.5194/acp-21-5983-2021.

Diemoz, H., Barnaba, F., Magri, T., Pession, G., Dionisi, D., Pittavino, S., Tombolato, I.K.F., Campanelli, M., Della Ceca, L.S., Hervo, M., Di Liberto, L., Ferrero, L., Gobbi, G.P., 2019. Transport of Po valley aerosol pollution to the northwestern Alps Part 1: phenomenology. Atmos. Chem. Phys. 19, 3065–3095. https://doi.org/10.5194/acp-19-3065-2019.

Diémoz, H., Paolo Gobbi, G., Magri, T., Pession, G., Pittavino, S., Tombolato, I.K.F., Campanelli, M., Barnaba, F., 2019. Transport of Po Valley aerosol pollution to the northwestern Alps-Part 2: long-term impact on air quality. Atmos. Chem. Phys. 19, 10129–10160. https://doi.org/10.5194/acp-19-10129-2019.

EC (European Commission), 2022. Proposal for a Directive of the European Parliament and of the Council on ambient air quality and cleaner air for Europe. COM(2022) 542 final/2, 2022/0347(COD). https://eur-lex.europa.eu/legal-content/EN/TXT/?uri=COM:2022:542:FIN. Accessed October 2023.

EEA (European Environment Agency), 2023a. Emissions of the main air pollutants in Europe. Indic. Assess. Data maps. https://www.eea.europa.eu/ims/emissions-of-the-main-air.

EEA (European Environmental Agency), 2020. Air quality in Europe - 2020 report. In: EEA Rep, vol. 162. Publications Office of the European Union, Luxembourg. https://doi.org/10.2800/786656.

EEA (European Environmental Agency), 2023b. Europe's air quality status 2023b. Briefing no. 05/2023, EN HTML: TH-AM-23-006-EN-Q. https://doi.org/10.2800/59526. ISBN: ISBN: 978-92-9480-554-6 - ISSN: 2467-3196.

Engelhart, G.J., Hildebrandt, L., Kostenidou, E., Mihalopoulos, N., Donahue, N.M., Pandis, S.N., 2011. Water content of aged aerosol. Atmos. Chem. Phys. 11, 911–920. https://doi.org/10.5194/acp-11-911-2011.

Ervens, B., Feingold, G., Frost, G.J., Kreidenweis, S.M., 2004. A modeling of study of aqueous production of dicarboxylic acids: 1. Chemical pathways and speciated organic mass production. J. Geophys. Res. D Atmos. 109 https://doi.org/10.1029/2003JD004387.

EU (European Union), 2008. Directive 2008/50/EC of the European Parliament and of the Council of 21 May 2008 on ambient air quality and cleaner air for Europe. Off. J. Eur. Union L 152, 1–44, 11.6.2008. http://data.europa.eu/eli/dir/2008/50/oj.

Fine, P.M., Cass, G.R., Simoneit, B.R.T., 2001. Chemical characterization of fine particle emissions from fireplace combustion of woods grown in the northeastern United States. Environ. Sci. Technol. 35, 2665–2675. https://doi.org/10.1021/es001466k.

Fussell, J.C., Franklin, M., Green, D.C., Gustafsson, M., Harrison, R.M., Hicks, W., Kelly, F.J., Kishta, F., Miller, M.R., Mudway, I.S., Oroumiyeh, F., Selley, L., Wang, M., Zhu, Y., 2022. A review of road traffic-derived non-exhaust particles: emissions, physicochemical characteristics, health risks, and mitigation measures. Environ. Sci. Technol. 56, 6813–6835. https://doi.org/10.1021/acs.est.2c01072.

Gilardoni, S., Massoli, P., Paglione, M., Giulianelli, L., Carbone, C., Rinaldi, M., Decesari, S., Sandrini, S., Costabile, F., Gobbi, G.P., Pietrogrande, M.C., Visentin, M., Scotto, F., Fuzzi, S., Facchini, M.C., 2016. Direct observation of aqueous secondary organic aerosol from biomass-burning emissions. Proc. Natl. Acad. Sci. U.S.A. 113, 10013–10018. https://doi.org/10.1073/pnas.1602212113.

Giovannini, L., Zardi, D., De Franceschi, M., Chen, F., 2014. Numerical simulations of boundary-layer processes and urban-induced alterations in an Alpine valley. Int. J. Climatol. 34, 1111–1131. https://doi.org/10.1002/joc.3750.

Gohm, A., Harnisch, F., Vergeiner, J., Obleitner, F., Schnitzhofer, R., Hansel, A., Fix, A., Neininger, B., Emeis, S., Schäfer, K., 2009. Air pollution transport in an Alpine valley: results from airborne and ground-based observations. Boundary-Layer Meteorol. 131, 441–463. https://doi.org/10.1007/s10546-009-9371-9.

Golly, B., Waked, A., Weber, S., Samake, A., Jacob, V., Conil, S., Rangognio, J., Chrétien, E., Vagnot, M.P., Robic, P.Y., Besombes, J.L., Jaffrezo, J.L., 2019. Organic markers and OC source apportionment for seasonal variations of PM2.5 at 5 rural sites in France. Atmos. Environ. 198, 142–157. https://doi.org/10.1016/j.atmosenv.2018.10.027.

Gregoris, E., Morabito, E., Barbaro, E., Feltracco, M., Toscano, G., Merico, E., Grasso, F. M., Cesari, D., Conte, M., Contini, D., Gambaro, A., 2021. Chemical characterization and source apportionment of size-segregated aerosol in the port-city of Venice (Italy). Atmos. Pollut. Res. 12, 261–271. https://doi.org/10.1016/j.apr.2020.11.007.

Hallquist, M., Wenger, J.C., Baltensperger, U., Rudich, Y., Simpson, D., Claeys, M., Dommen, J., Donahue, N.M., George, C., Goldstein, A.H., Hamilton, J.F., Herrmann, H., Hoffmann, T., Iinuma, Y., Jang, M., Jenkin, M.E., Jimenez, J.L., Kiendler-Scharr, A., Maenhaut, W., McFiggans, G., Mentel, T.F., Monod, A., Prévôt, A.S.H., Seinfeld, J.H., Surratt, J.D., Szmigielski, R., Wildt, J., 2009. The formation, properties and impact of secondary organic aerosol: current and emerging issues. Atmos. Chem. Phys. 9, 5155–5236. https://doi.org/10.5194/acp-9-5155-2009.

Hand, J.L., 2011. Spatial and seasonal patterns and temporal variability of haze and its constituents in the United States. Improve Report V. http://vista.cira.colostate.edu/Improve/spatial-and-seasonal-patterns-and-temporal-variability-of-haze-and-its-constituents-in-the-united-states-report-v-june-2011/.

Hopke, P.K., 2015. Applying multivariate curve resolution to source apportionment of the atmospheric aerosol. ACS Symp. Ser. 1199, 129–157. https://doi.org/10.1021/bk-2015-1199.ch006.

Hopke, P.K., 2016. Review of receptor modeling methods for source apportionment. J. Air Waste Manag. Assoc. 66, 237–259. https://doi.org/10.1080/10962247.2016.1140693.

INEMAR, 2022. Inventario Regionale delle Emissioni in Atmosfera in Veneto, Edizione 2019. ARPA Veneto - Dipartimento Regionale Qualità dell'Ambiente - Unità Organizzativa Qualità dell'Aria, Regione del Veneto - Area Tutela e Sicurezza del Territorio. Direzione Ambiente e Transizione Ecologica - UO Qualità dell'Aria e Tutela dell'Atmosfera. https://www.arpa.veneto.it/dati-ambientali/open-data/atmosfera/dati-comunali-emissioni-inemar-veneto.

Jayarathne, T., Stockwell, C.E., Yokelson, R.J., Nakao, S., Stone, E.A., 2014. Emissions of fine particle fluoride from biomass burning. Environ. Sci. Technol. 48, 12636–12644. https://doi.org/10.1021/es502933j.

Kawamura, K., Bikkina, S., 2016. A review of dicarboxylic acids and related compounds in atmospheric aerosols: molecular distributions, sources and transformation. Atmos. Res. 170, 140–160. https://doi.org/10.1016/j.atmosres.2015.11.018.

Kim, E., Hopke, P.K., Edgerton, E.S., 2003. Source identification of Atlanta aerosol by positive matrix factorization. J. Air Waste Manag. Assoc. 53, 731–739. https://doi.org/10.1080/10473289.2003.10466209.

Kley, D., Kleinmann, M., Sanderman, H., Krupa, S., 1999. Photochemical oxidants: state of the science. Environ. Pollut. 100, 19–42. https://doi.org/10.1016/S0269-7491(99)00086-X.

Kodros, J.K., Papanastasiou, D.K., Paglione, M., Masiol, M., Squizzato, S., Florou, K., Skyllakou, K., Kaltsonoudis, C., Nenes, A., Pandis, S.N., 2020. Rapid dark aging of biomass burning as an overlooked source of oxidized organic aerosol. Proc. Natl. Acad. Sci. U.S.A. 117, 33028–33033. https://doi.org/10.1073/PNAS.2010365117.

Kukkonen, J., López-Aparicio, S., Segersson, D., Geels, C., Kangas, L., Kauhaniemi, M., Maragkidou, A., Jensen, A., Assmuth, T., Karppinen, A., Sofiev, M., Hellén, H., Riikonen, K., Nikmo, J., Kousa, A., Niemi, J.V., Karvosenoja, N., Sousa Santos, G., Sundvor, I., Im, U., Christensen, J.H., Nielsen, O.K., Plejdrup, M.S., Klenø Nøjgaard, J., Omstedt, G., Andersson, C., Forsberg, B., Brandt, J., 2020. The influence of residential wood combustion on the concentrations of PM2.5 in four Nordic cities. Atmos. Chem. Phys. 20, 4333–4365. https://doi.org/10.5194/acp-20-4333-2020.

Kundu, S., Kawamura, K., Andreae, T.W., Hoffer, A., Andreae, M.O., 2010. Molecular distributions of dicarboxylic acids, ketocarboxylic acids and ?-dicarbonyls in biomass burning aerosols: implications for photochemical production and degradation in smoke layers. Atmos. Chem. Phys. 10, 2209–2225. https://doi.org/10.5194/acp-10-2209-2010.

Kuwata, M., Liu, Y., McKinney, K., Martin, S.T., 2015. Physical state and acidity of inorganic sulfate can regulate the production of secondary organic material from isoprene photooxidation products. Phys. Chem. Chem. Phys. 17, 5670–5678. https://doi.org/10.1039/c4cp04942j.

Lammel, G., Novák, J., Landlová, L., Dvorská, A., Klánová, J., upr, P., Kohoutek, J., Reimer, E., Škrdlíková, L., 2011. Sources and distributions of polycyclic aromatic hydrocarbons and toxicity of polluted atmosphere aerosols. In: Zereini, F., Wiseman, C. (Eds.), Urban Airborne Particulate Matter. Environ. Sci. Eng. Springer, Berlin, Heidelberg, pp. 39–62. https://doi.org/10.1007/978-3-642-12278-1_3.

Largeron, Y., Staquet, C., 2016. Persistent inversion dynamics and wintertime PM10 air pollution in Alpine valleys. Atmos. Environ. 135, 92–108. https://doi.org/10.1016/j.atmosenv.2016.03.045.

Lee, A.K.Y., Willis, M.D., Healy, R.M., Wang, J.M., Jeong, C.H., Wenger, J.C., Evans, G.J., Abbatt, J.P.D., 2016. Single-particle characterization of biomass burning organic aerosol (BBOA): evidence for non-uniform mixing of high molecular weight organics and potassium. Atmos. Chem. Phys. 16, 5561–5572. https://doi.org/10.5194/acp-16-5561-2016.

Lim, C.Y., Hagan, D.H., Coggon, M.M., Koss, A.R., Sekimoto, K., De Gouw, J., Warneke, C., Cappa, C.D., Kroll, J.H., 2019. Secondary organic aerosol formation from the laboratory oxidation of biomass burning emissions. Atmos. Chem. Phys. 19, 12797–12809. https://doi.org/10.5194/acp-19-12797-2019.

Marynowski, L., Simoneit, B.R.T., 2022. Saccharides in atmospheric particulate and sedimentary organic matter: status overview and future perspectives. Chemosphere 288. https://doi.org/10.1016/j.chemosphere.2021.132376.

Masiol, M., Formenton, G., Pasqualetto, A., Pavoni, B., 2013. Seasonal trends and spatial variations of PM10-bounded polycyclic aromatic hydrocarbons in Veneto Region, Northeast Italy. Atmos. Environ. 79, 811–821. https://doi.org/10.1016/j.atmosenv.2013.07.025.

Masiol, M., Squizzato, S., Ceccato, D., Rampazzo, G., Pavoni, B., 2012. Determining the influence of different atmospheric circulation patterns on PM10 chemical composition in a source apportionment study. Atmos. Environ. 63, 117–124. https://doi.org/10.1016/j.atmosenv.2012.09.025.

Masiol, M., Squizzato, S., Formenton, G., Harrison, R.M., Agostinelli, C., 2017. Air quality across a European hotspot: spatial gradients, seasonality, diurnal cycles and trends in the Veneto region, NE Italy. Sci. Total Environ. 576, 210–224. https://doi.org/10.1016/j.scitotenv.2016.10.042.

Masiol, M., Squizzato, S., Formenton, G., Khan, M.B., Hopke, P.K., Nenes, A., Pandis, S. N., Tositti, L., Benetello, F., Visin, F., Pavoni, B., 2020. Hybrid multiple-site mass closure and source apportionment of PM2.5 and aerosol acidity at major cities in the Po Valley. Sci. Total Environ. 704 https://doi.org/10.1016/j.scitotenv.2019.135287.

Masiol, M., Squizzato, S., Rampazzo, G., Pavoni, B., 2014. Source apportionment of PM2.5 at multiple sites in Venice (Italy): spatial variability and the role of weather. Atmos. Environ. 98, 78–88. https://doi.org/10.1016/j.atmosenv.2014.08.059.

Masiol, M., Benetello, F., Harrison, R.M., Formenton, G., De Gaspari, F., Pavoni, B., 2015. Spatial, seasonal trends and transboundary transport of $PM_{2.5}$ inorganic ions in the Veneto region (Northeastern Italy). Atmos. Environ. 117, 19–31. https://doi.org/10.1016/j.atmosenv.2015.06.044.

Orasche, J., Seidel, T., Hartmann, H., Schnelle-Kreis, J., Chow, J.C., Ruppert, H., Zimmermann, R., 2012. Comparison of emissions from wood combustion. Part 1: emission factors and characteristics from different small-scale residential heating appliances considering particulate matter and polycyclic aromatic hydrocarbon (PAH)-Related toxicological potential of particle-bound organic species. Energy Fuels 26, 6695–6704. https://doi.org/10.1021/ef301295k.

Paatero, P., 1997. Least squares formulation of robust non-negative factor analysis. Chemometr. Intell. Lab. Syst. 37, 23–35. https://doi.org/10.1016/S0169-7439(96)00044-5.

Paatero, P., Eberly, S., Brown, S.G., Norris, G.A., 2014. Methods for estimating uncertainty in factor analytic solutions. Atmos. Meas. Tech. 7, 781–797. https://doi.org/10.5194/amt-7-781-2014.

Paatero, P., Hopke, P.K., 2003. Discarding or downweighting high-noise variables in factor analytic models. Anal. Chim. Acta 490, 277–289. https://doi.org/10.1016/S0003-2670(02)01643-4.

Paatero, P., Hopke, P.K., Begum, B.A., Biswas, S.K., 2005. A graphical diagnostic method for assessing the rotation in factor analytical models of atmospheric pollution. Atmos. Environ. 39, 193–201. https://doi.org/10.1016/j.atmosenv.2004.08.018.

Paatero, P., Tapper, U., 1994. Positive matrix factorization: a non?negative factor model with optimal utilization of error estimates of data values. Environmetrics 5, 111–126. https://doi.org/10.1002/env.3170050203.

Pant, P., Harrison, R.M., 2013. Estimation of the contribution of road traffic emissions to particulate matter concentrations from field measurements: a review. Atmos. Environ. 77, 78–97. https://doi.org/10.1016/j.atmosenv.2013.04.028.

Pashynska, V., Vermeylen, R., Vas, G., Maenhaut, W., Claeys, M., 2002. Development of a gas chromatographic/ion trap mass spectrometric method for the determination of levoglucosan and saccharidic compounds in atmospheric aerosols. Application to urban aerosols. J. Mass Spectrom. 37, 1249–1257. https://doi.org/10.1002/jms.391.

Pathak, R.K., Wu, W.S., Wang, T., 2009. Summertime PM2.5 ionic species in four major cities of China: nitrate formation in an ammonia-deficient atmosphere. Atmos. Chem. Phys. 9, 1711–1722. https://doi.org/10.5194/acp-9-1711-2009.

Perrone, M.G., Larsen, B.R., Ferrero, L., Sangiorgi, G., De Gennaro, G., Udisti, R., Zangrando, R., Gambaro, A., Bolzacchini, E., 2012. Sources of high PM2.5 concentrations in Milan, Northern Italy: molecular marker data and CMB modelling. Sci. Total Environ. 414, 343–355. https://doi.org/10.1016/j.scitotenv.2011.11.026.

Pivato, A., Pegoraro, L., Masiol, M., Bortolazzo, E., Bonato, T., Formenton, G., Cappai, G., Beggio, G., Giancristofaro, R.A., 2023. Long time series analysis of air quality data in the Veneto region (Northern Italy) to support environmental policies. Atmos. Environ. 298 https://doi.org/10.1016/j.atmosenv.2023.119610.

Puxbaum, H., Caseiro, A., Sánchez-Ochoa, A., Kasper-Giebl, A., Claeys, M., Gelencsér, A., Legrand, M., Preunkert, S., Pio, C.A., 2007. Levoglucosan levels at background sites in Europe for assessing the impact of biomass combustion on the European aerosol background. J. Geophys. Res. Atmos. 112 https://doi.org/10.1029/2006JD008114.

Quayle, R.G., Diaz, H.F., 1980. Heating degree day data applied to residential heating energy consumption. J. Appl. Meteorol. Climatol. 19 (3), 241–246. https://doi.org/10.1175/1520-0450(1980)019%3C0241:HDDDAT%3E2.0.CO;2.

R Core Team, 2022. R: A Language and Environment for Statistical Computing. R Foundation for Statistical Computing, Vienna, Austria. URL. https://www.R-project.org/.

Rathnayake, C.M., Metwali, N., Jayarathne, T., Kettler, J., Huang, Y., Thorne, P.S., O'Shaughnessy, P.T., Stone, E.A., 2017. Influence of rain on the abundance of bioaerosols in fine and coarse particles. Atmos. Chem. Phys. 17, 2459–2475. https://doi.org/10.5194/acp-17-2459-2017.

Reff, A., Eberly, S.I., Bhave, P.V., 2007. Receptor modeling of ambient particulate matter data using positive matrix factorization: review of existing methods. J. Air Waste Manag. Assoc. 57, 146–154. https://doi.org/10.1080/10473289.2007.10465319.

Ricciardelli, I., Bacco, D., Rinaldi, M., Bonafè, G., Scotto, F., Trentini, A., Bertacci, G., Ugolini, P., Zigola, C., Rovere, F., Maccone, C., Pironi, C., Poluzzi, V., 2017. A three-year investigation of daily PM2.5 main chemical components in four sites: the routine measurement program of the Supersito Project (Po Valley, Italy). Atmos. Environ. 152, 418–430. https://doi.org/10.1016/j.atmosenv.2016.12.052.

Samaké, A., Jaffrezo, J.L., Favez, O., Weber, S., Jacob, V., Canete, T., Albinet, A., Charron, A., Riffault, V., Perdrix, E., Waked, A., Golly, B., Salameh, D., Chevrier, F., Miguel Oliveira, D., Besombes, J.L., Martins, J.M.F., Bonnaire, N., Conil, S., Guillaud, G., Mesbah, B., Rocq, B., Robic, P.Y., Hulin, A., Le Meur, S., Descheemaecker, M., Chretien, E., Marchand, N., Uzu, G., 2019. Arabitol, mannitol, and glucose as tracers of primary biogenic organic aerosol: the influence of environmental factors on ambient air concentrations and spatial distribution over France. Atmos. Chem. Phys. 19, 11013–11030. https://doi.org/10.5194/acp-19-11013-2019.

Schkolnik, G., Rudich, Y., 2006. Detection and quantification of levoglucosan in atmospheric aerosols: a review. Anal. Bioanal. Chem. 385, 26–33. https://doi.org/10.1007/s00216-005-0168-5.

Schmidl, C., Marr, I.L., Caseiro, A., Kotianová, P., Berner, A., Bauer, H., Kasper-Giebl, A., Puxbaum, H., 2008. Chemical characterisation of fine particle emissions from wood stove combustion of common woods growing in mid-European Alpine regions. Atmos. Environ. 42, 126–141. https://doi.org/10.1016/j.atmosenv.2007.09.028.

Scotto, F., Bacco, D., Lasagni, S., Trentini, A., Poluzzi, V., Vecchi, R., 2021. A multi-year source apportionment of PM2.5 at multiple sites in the southern Po Valley (Italy). Atmos. Pollut. Res. 12 https://doi.org/10.1016/j.apr.2021.101192.

Seinfeld, J.H., Pandis, S.N., 2016. Atmospheric chemistry and physics: from air pollution to climate change. In: Atmospheric Chemistry and Physics, third ed. John Wiley & Sons, New York, NY, USA. https://doi.org/10.1080/00139157.1999.10544295.

Shrivastava, M., Cappa, C.D., Fan, J., Goldstein, A.H., Guenther, A.B., Jimenez, J.L., Kuang, C., Laskin, A., Martin, S.T., Ng, N.L., Petaja, T., Pierce, J.R., Rasch, P.J., Roldin, P., Seinfeld, J.H., Shilling, J., Smith, J.N., Thornton, J.A., Volkamer, R., Wang, J., Worsnop, D.R., Zaveri, R.A., Zelenyuk, A., Zhang, Q., 2017. Recent advances in understanding secondary organic aerosol: implications for global climate forcing. Rev. Geophys. 55, 509–559. https://doi.org/10.1002/2016RG000540.

Simoneit, B.R.T., 2002. Biomass burning - a review of organic tracers for smoke from incomplete combustion. Appl. Geochem. 17, 129–162. https://doi.org/10.1016/S0883-2927(01)00061-0.

Sofowote, U.M., Healy, R.M., Su, Y., Debosz, J., Noble, M., Munoz, A., Jeong, C.H., Wang, J.M., Hilker, N., Evans, G.J., Brook, J.R., Lu, G., Hopke, P.K., 2021. Sources, variability and parameterizations of intra-city factors obtained from dispersion-normalized multi-time resolution factor analyses of PM2.5 in an urban environment. Sci. Total Environ. 761 https://doi.org/10.1016/j.scitotenv.2020.143225.

Song, W., Liu, X.Y., 2023. Source oxygen contributions of primary nitrate emitted from biomass burning. Sci. Total Environ. 854 https://doi.org/10.1016/j.scitotenv.2022.158736.

Spinoni, J., Vogt, J.V., Barbosa, P., Dosio, A., McCormick, N., Bigano, A., Füssel, H.M., 2018. Changes of heating and cooling degree-days in Europe from 1981 to 2100. Int. J. Climatol. 38, e191–e208. https://doi.org/10.1002/joc.5362.

Spinoni, J., Vogt, J., Barbosa, P., 2015. European degree-day climatologies and trends for the period 1951-2011. Int. J. Climatol. 35, 25–36. https://doi.org/10.1002/joc.3959.

Squizzato, S., Cazzaro, M., Innocente, E., Visin, F., Hopke, P.K., Rampazzo, G., 2017. Urban air quality in a mid-size city - PM2.5 composition, sources and identification of impact areas: from local to long range contributions. Atmos. Res. 186, 51–62. https://doi.org/10.1016/j.atmosres.2016.11.011.

Squizzato, S., Masiol, M., Agostini, C., Visin, F., Formenton, G., Harrison, R.M., Rampazzo, G., 2016. Factors, origin and sources affecting PM1 concentrations and composition at an urban background site. Atmos. Res. 180, 262–273. https://doi.org/10.1016/j.atmosres.2016.06.002.

Squizzato, S., Masiol, M., Brunelli, A., Pistollato, S., Tarabotti, E., Rampazzo, G., Pavoni, B., 2013. Factors determining the formation of secondary inorganic aerosol: a case study in the Po Valley (Italy). Atmos. Chem. Phys. 13, 1927–1939. https://doi.org/10.5194/acp-13-1927-2013.

Stortini, A.M., Freda, A., Cesari, D., Cairns, W.R.L., Contini, D., Barbante, C., Prodi, F., Cescon, P., Gambaro, A., 2009. An evaluation of the PM2.5 trace elemental composition in the Venice Lagoon area and an analysis of the possible sources. Atmos. Environ. 43, 6296–6304. https://doi.org/10.1016/j.atmosenv.2009.09.033.

Thom, H.C.S., 1954. The rational relationship between heating degree days and temperature. Mon. Weather Rev. 82 (1), 1–6. https://doi.org/10.1175/1520-0493(1954)082%3C0001:TRRBHD%3E2.0.CO;2.

Turnock, S.T., Butt, E.W., Richardson, T.B., Mann, G.W., Reddington, C.L., Forster, P.M., Haywood, J., Crippa, M., Janssens-Maenhout, G., Johnson, C.E., Bellouin, N., Carslaw, K.S., Spracklen, D.V., 2016. The impact of European legislative and technology measures to reduce air pollutants on air quality, human health and climate. Environ. Res. Lett. 11, 024010 https://doi.org/10.1088/1748-9326/11/2/024010.

Vicente, E.D., Alves, C.A., 2018. An overview of particulate emissions from residential biomass combustion. Atmos. Res. 199, 159–185. https://doi.org/10.1016/j.atmosres.2017.08.027.

Vicente, E.D., Duarte, M.A., Tarelho, L.A.C., Nunes, T.F., Amato, F., Querol, X., Colombi, C., Gianelle, V., Alves, C.A., 2015. Particulate and gaseous emissions from the combustion of different biofuels in a pellet stove. Atmos. Environ. 120, 15–27. https://doi.org/10.1016/j.atmosenv.2015.08.067.

Wan, X., Kang, S., Rupakheti, M., Zhang, Q., Tripathee, L., Guo, J., Chen, P., Rupakheti, D., Panday, A.K., Lawrence, M.G., Kawamura, K., Cong, Z., 2019. Molecular characterization of organic aerosols in the Kathmandu Valley, Nepal: insights into primary and secondary sources. Atmos. Chem. Phys. 19, 2725–2747. https://doi.org/10.5194/acp-19-2725-2019.

Whiteman, C.D., 2000. Mountain Meteorology: Fundamentals and Applications. Oxford University Press.

Whiteman, C.D., Bian, X., Zhong, S., 1999. Wintertime evolution of the temperature inversion in the Colorado Plateau Basin. J. Appl. Meteorol. 38, 1103–1117. https://doi.org/10.1175/1520-0450(1999)038<1103:WEOTTI>2.0.CO;2.

WHO (World Health Organization), 2021. WHO Global Air Quality Guidelines: Particulate Matter (?PM2.5 and PM10)?, Ozone, Nitrogen Dioxide, Sulfur Dioxide and Carbon Monoxide. World Health Organization. https://iris.who.int/handle/10665/345329.

WHO (World Health Organization, 2006. WHO Air quality guidelines for particulate matter, ozone, nitrogen dioxide and sulfur dioxide: global update 2005 : summary of risk assessment. World Health Organization, Occupational and Environmental Health Team. https://iris.who.int/handle/10665/69477.

Xu, J., Jia, C., He, J., Xu, H., Tang, Y.T., Ji, D., Yu, H., Xiao, H., Wang, C., 2019. Biomass burning and fungal spores as sources of fine aerosols in Yangtze River Delta, China - using multiple organic tracers to understand variability, correlations and origins. Environ. Pollut. 251, 155–165. https://doi.org/10.1016/j.envpol.2019.04.090.

Xu, J., Tian, Y., Cheng, C., Wang, C., Lin, Q., Li, M., Wang, X., Shi, G., 2020a. Characteristics and source apportionment of ambient single particles in Tianjin, China: the close association between oxalic acid and biomass burning. Atmos. Res. 237 https://doi.org/10.1016/j.atmosres.2020.104843.

Xu, S., Ren, L., Lang, Y., Hou, S., Ren, H., Wei, L., Wu, L., Deng, J., Hu, W., Pan, X., Sun, Y., Wang, Z., Su, H., Cheng, Y., Fu, P., 2020b. Molecular markers of biomass burning and primary biological aerosols in urban Beijing: Size distribution and seasonal variation. Atmos. Chem. Phys. 20, 3623–3644. https://doi.org/10.5194/acp-20-3623-2020.

Yang, C., Zhou, S., Zhang, C., Yu, M., Cao, F., Zhang, Y., 2022. Atmospheric chemistry of oxalate: insight into the role of relative humidity and aerosol acidity from high-resolution observation. J. Geophys. Res. Atmos. 127 https://doi.org/10.1029/2021JD035364.

Yazdani, A., Takahama, S., Kodros, J.K., Paglione, M., Masiol, M., Squizzato, S., Florou, K., Kaltsonoudis, C., Jorga, S.D., Pandis, S.N., Nenes, A., 2023. Chemical evolution of primary and secondary biomass burning aerosols during daytime and nighttime. Atmos. Chem. Phys. 23, 7461–7477. https://doi.org/10.5194/acp-23-7461-2023.

Yttri, K.E., Dye, C., Kiss, G., 2007. Ambient aerosol concentrations of sugars and sugar-alcohols at four different sites in Norway. Atmos. Chem. Phys. 7, 4267–4279. https://doi.org/10.5194/acp-7-4267-2007.

Yttri, K.E., Simpson, D., Bergström, R., Kiss, G., Szidat, S., Ceburnis, D., Eckhardt, S., Hueglin, C., Nøjgaard, J.K., Perrino, C., Pisso, I., Prevot, A.S.H., Putaud, J.P., Spindler, G., Vana, M., Zhang, Y.L., Aas, W., 2019. The EMEP Intensive Measurement Period campaign, 2008-2009: characterizing carbonaceous aerosol at nine rural sites in Europe. Atmos. Chem. Phys. 19, 4211–4233. https://doi.org/10.5194/acp-19-4211-2019.

Zhang, G., Lin, Q., Peng, L., Yang, Y., Fu, Y., Bi, X., Li, M., Chen, D., Chen, J., Cai, Z., Wang, X., Peng, P., Sheng, G., Zhou, Z., 2017. Insight into the in-cloud formation of oxalate based on in situ measurement by single particle mass spectrometry. Atmos. Chem. Phys. 17, 13891–13901. https://doi.org/10.5194/acp-17-13891-2017.

Zhang, L., Yang, L., Zhou, Q., Zhang, X., Xing, W., Wei, Y., Hu, M., Zhao, L., Toriba, A., Hayakawa, K., Tang, N., 2020. Size distribution of particulate polycyclic aromatic hydrocarbons in fresh combustion smoke and ambient air: a review. J. Environ. Sci. (China) 88, 370–384. https://doi.org/10.1016/j.jes.2019.09.007.

Zhang, Y., Obrist, D., Zielinska, B., Gertler, A., 2013. Particulate emissions from different types of biomass burning. Atmos. Environ. 72, 27–35. https://doi.org/10.1016/j.atmosenv.2013.02.026.

Zhou, Y., Huang, X.H., Bian, Q., Griffith, S.M., Louie, P.K.K., Yu, J.Z., 2015. Sources and atmospheric processes impacting oxalate at a suburban coastal site in Hong Kong: insights inferred from 1year hourly measurements. J. Geophys. Res. 120, 9772–9788. https://doi.org/10.1002/2015JD023531.

Zíková, N., Wang, Y., Yang, F., Li, X., Tian, M., Hopke, P.K., 2016. On the source contribution to Beijing PM2.5 concentrations. Atmos. Environ. 134, 84–95. https://doi.org/10.1016/j.atmosenv.2016.03.047.